





Article

Novel Tricarbonylrhenium-Anthrapyrazole Complexes with DNA-Binding and Antitumor Properties: In Vitro and In Vivo Pharmacokinetic Studies with ^{99m}Tc -Analogue

Georgios Paparidis ¹, Melpomeni Akrivou ², George Psomas ³ , Ioannis S. Vizirianakis ^{2,4} ,
Antonios Hatzidimitriou ³, Catherine Gabriel ^{5,6} , Dimosthenis Sarigiannis ^{5,6} and Dionysia Papagiannopoulou ^{1,*} 

¹ Laboratory of Pharmaceutical Chemistry, School of Pharmacy, Faculty of Health Sciences, Aristotle University of Thessaloniki, 54124 Thessaloniki, Greece

² Laboratory of Pharmacology, School of Pharmacy, Faculty of Health Sciences, Aristotle University of Thessaloniki, 54124 Thessaloniki, Greece

³ Department of General and Inorganic Chemistry, Faculty of Chemistry, Aristotle University of Thessaloniki, 54124 Thessaloniki, Greece

⁴ Department of Health Sciences, School of Life & Health Sciences, University of Nicosia, Nicosia 2417, Cyprus

⁵ Environmental Engineering Laboratory, Department of Chemical Engineering, Aristotle University of Thessaloniki, 54124 Thessaloniki, Greece

⁶ HERACLES Research Center on the Exposome and Health, Center for Interdisciplinary Research and Innovation, Balkan Center, Bldg. B, 10th km Thessaloniki-Thermi Road, 57001 Thessaloniki, Greece

* Correspondence: papagd@pharm.auth.gr

Abstract: Organometallic complexes of *fac*-tricarbonylrhenium have been shown to exhibit anticancer properties. Anthrapyrazole anticancer agents act as DNA intercalators and topoisomerase II α inhibitors, leading to double-strand breaks (DBS) and cell cycle arrest. This work involves the synthesis and biological evaluation of novel *fac*-tricarbonyl-rhenium complexes with anthrapyrazole derivatives. The anthrapyrazole moiety was synthesized from 1,8-dihydroxyanthraquinone, and three ligands **L1**, **L2** and **L3** were prepared. Ligand **L1** coordinates via the phenolic O and pyrazole N as bidentate chelator forming the *fac*-[Re(CO)₃(κ^2 -N,O)(MeOH)]-type complex, **ReL1**. Ligand **L2** contains a pendant picolylamine N,N'-chelating system, forming the bidentate *fac*-[Re(CO)₃(κ^2 -N,N')Br]-type complex, **ReL2**. Ligand **L3** contains a pendant picolylaminomonoacetic acid chelating system, forming a tridentate *fac*-[Re(CO)₃(κ^3 -N,N',O)]-type complex, **ReL3**. Complex **ReL4** contains a picolylamine chelator, forming a complex with structure *fac*-[Re(CO)₃(κ^2 -N,N')Br], which was synthesized as a model for **ReL2**, and its coordination mode was resolved by X-ray crystallography. The complexes were characterized spectroscopically, and their biological properties were evaluated in vitro, in terms of DNA binding as well as for the cytotoxicity against CT-26 tumor cell line. Tumor cell cytotoxicity was high for ligand **L2** and complex **ReL2**, exhibiting IC₅₀ values of 0.36 and 0.64 μM , respectively. The most promising complex **ReL2** was evaluated further by the preparation of its congener γ -emitting technetium-99m radio-complex, $^{99m}\text{TcL2}$. The in vitro uptake in CT26 tumor cells and the in vivo uptake in CT26 tumor-bearing mice of $^{99m}\text{TcL2}$ was determined, and its pharmacokinetic profile was established. These data indicate that the ^{99m}Tc complex has suitable properties to enter tumor cells in vitro and in vivo, and therefore **ReL2** is promising for further evaluation.

Keywords: rhenium; tricarbonylrhenium; anthrapyrazole; anthraquinone; DNA-binding studies; cytotoxicity; technetium-99m



Citation: Paparidis, G.; Akrivou, M.; Psomas, G.; Vizirianakis, I.S.; Hatzidimitriou, A.; Gabriel, C.; Sarigiannis, D.; Papagiannopoulou, D. Novel Tricarbonylrhenium-Anthrapyrazole Complexes with DNA-Binding and Antitumor Properties: In Vitro and In Vivo Pharmacokinetic Studies with ^{99m}Tc -Analogue. *Inorganics* **2024**, *12*, 254. <https://doi.org/10.3390/inorganics12090254>

Academic Editor: Vinay K. Sharma

Received: 19 August 2024

Revised: 6 September 2024

Accepted: 19 September 2024

Published: 21 September 2024



Copyright: © 2024 by the authors. Licensee MDPI, Basel, Switzerland. This article is an open access article distributed under the terms and conditions of the Creative Commons Attribution (CC BY) license (<https://creativecommons.org/licenses/by/4.0/>).

1. Introduction

The development of metal complexes in therapeutics, especially in the treatment of cancer, has made significant advances to date [1–7]. Platinum-based drugs have been used as first-line anticancer agents for half a century now [8]. In this area of research,

organometallic complexes of *fac*-tricarbonylrhenium have attracted attention in terms of their potential pharmaceutical applications for the development of novel antitumor and antimicrobial agents, as well as of luminescent probes for optical imaging [9–13]. The utilization of the *fac*-tricarbonylrhenium core is attractive for pharmaceutical applications due to its thermodynamic and kinetic stability, as well as for its versatility in drug design, with the existence of a variety of suitable chelating strategies. In addition, a number of research results show strong biological properties, which warrants their future exploration [13].

DNA intercalators are small molecules that can reversibly bind in between adjacent base pairs of double-stranded DNA (dsDNA). By binding to DNA, intercalators may cause fatal perturbations in essential DNA-associated processes such as replication, transcription and repair. Such polyaromatic frameworks include anthracenes, acridines, anthraquinones, phenazines, quinolones, phenanthridines, etc. [14]. Metal complexes may also intercalate with nucleic acid sequences either by conjugation to an organic intercalator or by coordination with a suitable chelating system, also known in the literature as metallointercalators, containing phenanthroline, phenanthrenequinone diimine and other ligands with extended aromatic systems [15]. Tricarbonylrhenium complexes with polyaromatic ligands such as phenanthrolines [16], quinolones [17] and bipyridine [18] have also been reported as antitumor agents.

Drug molecules containing the anthraquinone group are known to have clinical applications in therapeutic regimens against cancer. The anthraquinone scaffold provides flatness, due to the aromatic polycyclic system, causing intercalation between the double helix of DNA and the inhibition of topoisomerase II enzyme. Anthraquinone-based antitumor cytotoxic agents such as daunorubicin, doxorubicin, mitoxantrone and pixantrone, used in tumor therapy, are both Topo-II inhibitors and intercalators [19,20]. In this light, Imstepf et al. developed tricarbonylrhenium-doxorubicin complexes that were evaluated for their ability to inhibit Topo-II α [21].

The anthraquinone scaffold participates in redox processes, leading to the production of free radicals, which enhances the cytotoxic profile of the compound in both cancer and normal cells. The cardiotoxicity of anthraquinone derivatives led to the design and development of an alternative scaffold [22]. Anthrapyrazoles, such as losoxantrone, contain a pyrazole ring in the chromophore site instead of the quinone group, and they exhibit significantly reduced cardiotoxicity, as shown in preclinical and clinical studies [23].

In this work, we developed new anthrapyrazole-based ligands suitable for complexation with tricarbonylrhenium as potential antitumor agents, taking into consideration the reduced cardiotoxicity as well as the presence of coordinating atoms in this moiety. Therefore, we designed ligands to coordinate with *fac*-tricarbonylrhenium core either directly with the (N,O)-donor atoms of the anthrapyrazole pharmacophore, ligand **L1** or indirectly via the pendant bidentate (N,N)- and tridentate (N,N,O)-donor atom systems, ligands **L2** and **L3**, respectively (Figure 1). The ligands and the rhenium complexes were evaluated in vitro for their ability to interact with calf-thymus (CT) DNA as well as for their cytotoxic properties in a tumor cell line. Complex **ReL2**, which exhibited the best biological properties, was translated to the analogous γ -emitting $^{99m}\text{TcL2}$ complex, which was evaluated in vitro and in vivo for its tumor uptake and distribution properties. Also, in order to simulate the structure of **ReL2**, the model complex **ReL4**, which also contains a picolylamine chelator and shares the same coordination mode of *fac*-[Re(CO) $_3$ (κ^2 -N,N')Br], was synthesized and characterized by X-ray crystallography.

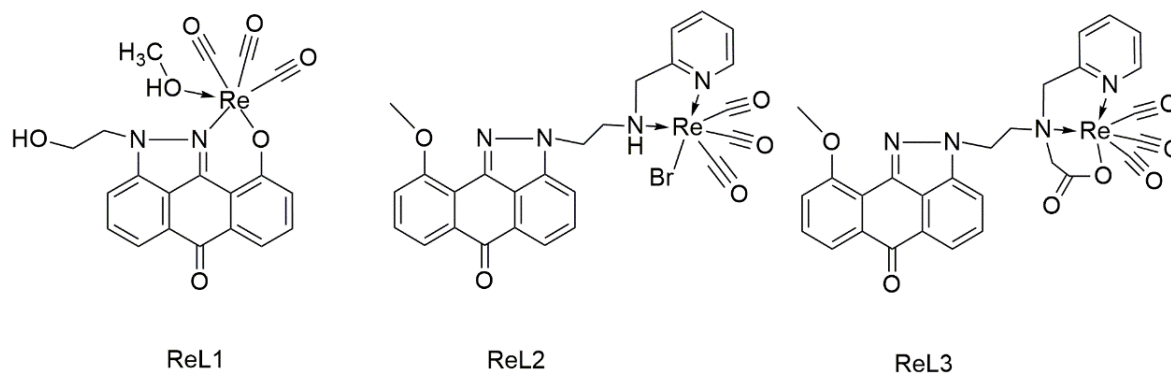
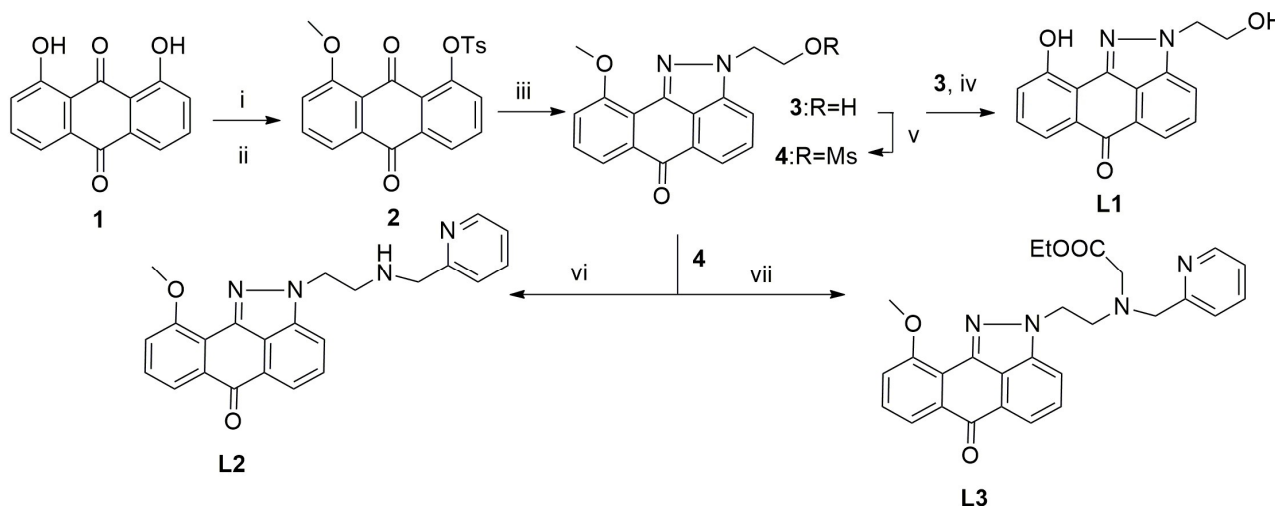


Figure 1. Structures of rhenium anthrapyrazole complexes.

2. Results and Discussion

2.1. Synthesis and Spectroscopic Characterization of Rhenium Complexes

Synthesis of the ligands **L1**, **L2** and **L3** followed the route depicted in Scheme 1. The intermediate compound **3** was synthesized according to methods reported in the literature for similar anthraquinones [24].

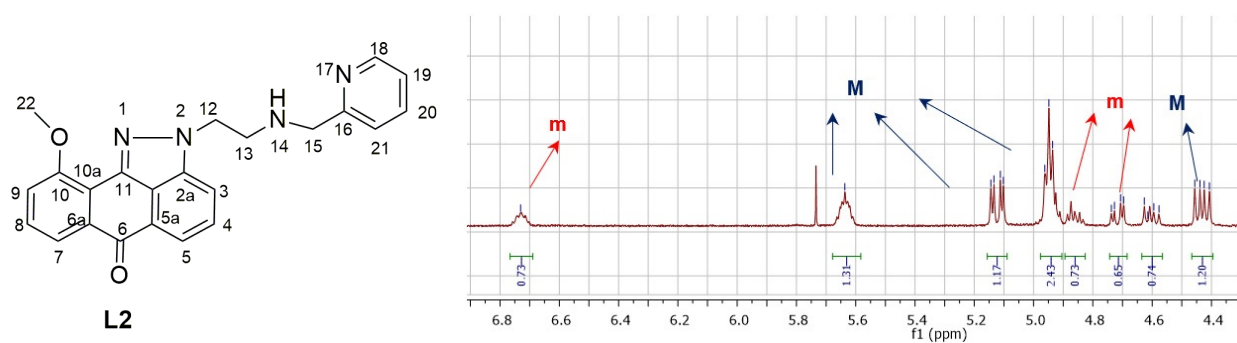


Scheme 1. (i) Me_2SO_4 , 60 °C; (ii) p-toluenesulfonyl chloride (TsCl), 60 °C (46%); (iii) 2-hydroxyethylhydrazine, 130 °C (25%); (iv) BBr_3 , 25 °C (65%); (v) methylsulfonyl chloride (MsCl), 25 °C (85%); (vi) 2-picolylamine, 65 °C (39%); (vii) ethyl 2-((pyridin-2-ylmethyl)amino)acetate, 80 °C (67%).

The bidentate ligand **L1** was prepared after the demethylation of **3** with BBr_3 . **L1** offers a bidentate N,O-donor system for direct complexation of the phenolic O and pyrazole N with tricarbonylrhenium. The complex was prepared by reaction of **L1** with equimolar amounts of the precursor $[\text{Re}(\text{CO})_5\text{Br}]$ in refluxing methanol for 24 h. The product was isolated by column chromatography as a red solid in average yield. The NMR analysis of the complex and the free ligand shows analogous proton and carbon signals, where in the $^1\text{H-NMR}$ spectrum of the complex, the phenolic proton signal of **L1** at 9.87 ppm is absent, and in the $^{13}\text{C-NMR}$ spectrum, the carbon of the C=N pyrazole ring is downfield-shifted to 160.30 ppm versus 154.43 ppm of **L1**. Furthermore, three CO carbons of the tricarbonylrhenium core appear at 197.89, 197.35 and 196.83 ppm. These NMR signals indicate the N,O-coordination of the metal core. The IR spectrum of the complex exhibits the characteristic bands of the ligand and a CO stretch at 2025, 1930 and 1900 cm^{-1} of the asymmetric tricarbonylrhenium core. High-resolution mass analysis revealed a signal that corresponded to negative molecular ions at m/z 579.0101 (60%) and 581.0139 (100%) for a $[\text{M}-\text{H}]^-$ pattern that matches the calculated values for $\text{M} = \text{C}_{20}\text{H}_{15}\text{N}_2\text{O}_7\text{Re}$ and corresponds to the formula $\text{fac-}[\text{Re}(\text{CO})_3(\kappa^2\text{-L1})(\text{MeOH})]$, as shown in Figure 1.

Ligands **L2** and **L3** were synthesized after the mesylation of the intermediate compound **3** and reaction of the mesylate compound **4** with the bidentate chelator 2-picolyamine to form **L2** or the tridentate chelator ethyl 2-((pyridin-2-ylmethyl)amino)acetate to form **L3**. These ligands were designed as part of the pendant approach, where metal complexation takes place with donor atoms that do not belong to the anthrapyrazole moiety.

L2 offers a bidentate N,N'-donor system from 2-picolyamine moiety for complexation with tricarbonylrhenium. The complex was prepared by reaction of **L2** with equimolar amounts of the precursor $[\text{Re}(\text{CO})_5\text{Br}]$ in refluxing methanol for 3 h. The product precipitated from the reaction mixture as a yellow solid in average yield. The NMR analysis of the complex shows the presence of two diastereomers due to the pseudooctahedral rhenium coordination and the prochiral secondary amine nitrogen donor. The ratio of the isomers is approximately 60:40, based on NMR and HPLC integration of the signals. In the ^1H -NMR spectrum of the complex, differences in the shifts of the two isomers were detected, some of which are shown in Figure 2. In particular, both isomers exhibit the characteristic pattern of (N,N') coordination due to picolyamine fragment, where the 2 protons of H-15 are split in two dd signals; in addition, the N-H can be observed at 5.64 and 6.73 ppm, respectively.



	L2	ReL2 (Major)	ReL2 (minor)
H-14	-	5.64 (m)	6.73 (m)
H-15	3.98 (s)	5.12 (dd, $J = 15.9, 5.2$ Hz), 4.43 (dd, $J = 15.9, 8.8$ Hz)	4.72 (dd, $J = 15.6, 5.3$ Hz), 4.60 (dd, $J = 15.7, 8.8$ Hz)
H-18	8.48 (d, $J = 4.6$ Hz)	8.78 (d, $J = 5.1$ Hz)	8.79 (d, $J = 5.1$ Hz)
H-19	7.12 (t, $J = 6.1$ Hz)	7.56 (t, $J = 7.7$ Hz)	7.48 (m)
H-20	7.58 (t, $J = 7.6$ Hz)	8.10 (td, $J = 7.8, 1.5$ Hz)	8.06 (td, $J = 7.8, 1.5$ Hz)
H-21	7.25 (d, $J = 8.1$ Hz)	7.79 (m)	7.68 (d, $J = 7.9$ Hz)

Figure 2. Representative section of the ^1H NMR spectrum of **ReL2** and table with proton shifts δ (in ppm) of **L2** (CDCl_3) and **ReL2** (d_6 -DMSO); isomer designation M: major (blue), m: minor (red).

In the ^{13}C -NMR spectrum, the CO signals of the tricarbonylrhenium core exhibit shifts at 197.89, 197.35 and 196.83 ppm. The IR spectrum of the complex exhibits the characteristic bands of the ligand and in addition the CO stretch at 2021, 1909 and 1867 cm^{-1} of the asymmetric tricarbonylrhenium core. The NMR and IR signals are in agreement with a *fac*- $[\text{Re}(\text{CO})_3(\text{N},\text{N}')\text{Br}]$ coordination mode. Furthermore, the high-resolution mass analysis revealed a signals that correspond to positive molecular ions $[\text{M} - \text{Br} + \text{DMSO}]^+$ at m/z 731.0995 (60%), 733.1125 (100%). Diastereomeric tricarbonylrhenium complexes have been synthesized previously by our group and others in the literature [25–28].

L3 offers a tridentate N,N',O-donor system of 2-((pyridin-2-ylmethyl)amino)acetate moiety for complexation with tricarbonylrhenium. The complex was prepared by reaction of **L3** with equimolar amounts of the precursor *fac*- $[\text{Re}(\text{CO})_3(\text{MeOH})_3](\text{OTf})$ in refluxing methanol for 24 h. The product was isolated by precipitation from methanol as a yellow solid in average yield. The NMR analysis of the complex and the free ligand shows analogous proton and carbon signals, where in the ^1H -NMR spectrum of the complex the characteristic pattern of this N,N',O-coordination is evident as the methylene protons

next to pyridine appear two doublets at 4.85 ppm ($J = 15.7$ Hz) and 3.59 ppm ($J = 16.6$ Hz), respectively, and the acetate protons appear as two doublets at 4.28 ppm ($J = 13.8$ Hz) and 4.16 ppm ($J = 13.3$ Hz), respectively. Furthermore, in the ^{13}C -NMR spectrum, the CO carbons of the tricarbonylrhenium core appear at 198.00 and 197.34 ppm. These NMR signals indicate the $[\text{N},\text{N}',\text{O}]$ coordination of the metal core. The IR spectrum of the complex exhibits the characteristic bands of the ligand, with the exception of the carboxylate ester stretch at 1737 cm^{-1} of the ligand and in addition the CO stretch at 2023, 1912 and 1870 cm^{-1} of the asymmetric tricarbonylrhenium core. High-resolution mass analysis revealed a signal that corresponds to positive molecular ions at m/z 711.1006 (60%) and 713.1050 (100%) for an $[\text{M} + \text{H}]^+$ pattern that matches the calculated values for $\text{M} = \text{C}_{28}\text{H}_{21}\text{N}_4\text{O}_7\text{Re}$ and corresponds to the formula $\text{fac-}[\text{Re}(\text{CO})_3(\kappa^3\text{-L3})]$, as shown in Figure 1.

Complex $\text{fac-}[\text{Re}(\text{CO})_3\text{Br}(\text{L4})]$ (Figure 3) was synthesized from **L4** (synthesis is reported in Supplementary File, ESI: 1. Synthesis of Ligand **L4**) under the same conditions employed for **ReL2** and was used as a model compound to corroborate the coordination mode of **ReL2**, which also contains a picolyamine chelator and shares the same coordination mode of $\text{fac-}[\text{Re}(\text{CO})_3(\kappa^2\text{-N},\text{N}')\text{Br}]$. The complex was crystallized, and its structure was solved by X-ray crystallography. The IR and NMR characterization of **ReL4** shows similar spectroscopic data with **ReL2** such as the stretching frequencies of the carbon monoxide coordinated to Re(I), which is 2021, 1913, 1875 cm^{-1} for **ReL4** vs. 2021, 1909, 1867 cm^{-1} of **ReL2**. In the ^{13}C -NMR spectrum, the CO signals of the tricarbonylrhenium core of **ReL4** exhibit shifts at 196.40, 195.47, 191.60 ppm, similar to those of **ReL2**, indicating that the coordination of the two complexes is the same.

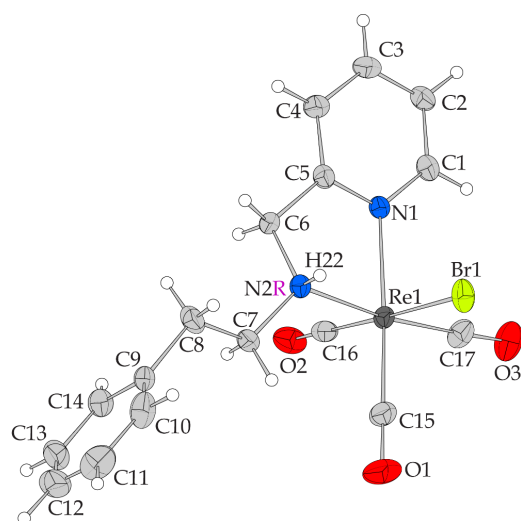


Figure 3. ORTEP of $\text{fac-}[\text{Re}(\text{CO})_3\text{Br}(\text{L4})]$ R-conformer.

2.2. X-ray-Structure

A plot of the molecular structure of complex $\text{fac-}[\text{Re}(\text{CO})_3\text{Br}(\text{L4})]$ is depicted in Figure 3, and bond distances and angles are shown in Table 1. The compound crystallizes in the monoclinic space group $P2_1/c$, and four neutral independent complex molecules can be found in the unit cell. The complex is mononuclear, and the coordination geometry is distorted octahedral. **L4** behaves as a bidentate ligand coordinated to rhenium(I) via the aromatic nitrogen atom N(1) and the amine nitrogen atom N(2), forming a five-membered chelate ring. Additionally, three carbon monoxide molecules are coordinated to Re(I) via the carbon atoms C(15), C(16), C(17) in facial orientation. The total coordination number of 6 is completed with the coordination of the bromine anion Br(1). The complex presents chirality on N(2) and from the four symmetrically equivalent molecules present in the unit cell, two of them are R type enantiomers, while the rest two are S conformers. In the ESI, we give both the cif files of the enantiomers and the plots of these isomers for comparison

(S conformer Figure S1). The bond distances and angles of complex *fac*-[Re(CO)₃Br(L4)] are similar to those found in other structures of rhenium(I)-tricarbonyl halide complexes coordinated to bidentate (N,N) donor ligands and forming five-membered ring, such as N,N'-bipyridine, pyridylimine and pyridylamine ligands [29–32].

Table 1. Selected geometric parameters (Å, °).

Re1—Br1	2.6219 (7)
Re1—N1	2.171 (4)
Re1—N2	2.223 (4)
Re1—C15	1.919 (6)
Re1—C16	1.894 (7)
Re1—C17	1.897 (6)
O1—C15	1.140 (8)
O2—C16	1.127 (7)
O3—C17	1.156 (7)
N1—C1	1.342 (7)
N1—C5	1.346 (7)
N2—C6	1.469 (7)
N2—C7	1.505 (7)
Br1—Re1—N1	85.82 (12)
Br1—Re1—N2	84.56 (12)
N1—Re1—N2	75.39 (16)
Br1—Re1—C15	92.5 (2)
N1—Re1—C15	174.8 (2)
N2—Re1—C15	99.5 (2)
Br1—Re1—C16	178.08 (18)
N1—Re1—C16	93.1 (2)
N2—Re1—C16	93.6 (2)
C15—Re1—C16	88.5 (3)
Br1—Re1—C17	91.2 (2)
N1—Re1—C17	98.5 (2)
N2—Re1—C17	172.8 (2)
C15—Re1—C17	86.5 (3)
C16—Re1—C17	90.5 (3)

In order to compare the distortion of the coordination octahedron of *fac*-[Re(CO)₃Br(L4)] with the reported analog [Re(CO)₃Br(L)] complexes, we used Octadist software version 3.1.0 [33] to compute the values of ζ and Σ (=deviations of the metal ion complex from an ideal octahedral structure) and Θ (=distortion from a perfect octahedral (O_h) to a trigonal prismatic (D_{3h}) geometry). The parameter ζ is the average of the sum of the deviation of six unique metal–ligand bond lengths around the central metal atom (d_i) from the average value (d_{mean}). The parameter Σ is the sum of the deviation of 12 unique cis ligand–metal–ligand angles (ϕ_i) from 90°. The parameter Θ is defined as the degree of trigonal distortion of the coordination geometry from an octahedron towards a trigonal prism. The Θ parameter is the sum of the deviation of 24 unique torsional angles between the ligand atoms on opposite triangular faces of the octahedron viewed along the pseudo-threefold axis (θ_i) from 60°. Comparison results are included in Table S1. From these results, it is concluded that [Re(CO)₃Br(L4)] presents nearly the same coordination parameters and distortion with the analog octahedral complexes already published. The pyridine rings of neighboring complexes have a centroid-to-centroid distance of 3.986 Å indicating weak π – π interactions present in the crystal structure of [Re(CO)₃Br(L4)], which give extra stability to the complex structure.

2.3. DNA-Binding Studies

The study of the interaction of anthrapyrazoles and their rhenium complexes with DNA is of great interest due to their ability to act as DNA intercalators. Interactions between a compound and CT DNA may cause changes to the absorption bands upon addition of

CT DNA in various ratios (r) values ($=[\text{compound}]/[\text{DNA}]$). The UV-vis spectra of the anthrapyrazoles and their complexes in DMSO in the presence of increasing amounts of CT DNA are shown in Figure 4 and Figure S2. The UV-vis spectra of the compounds exhibited similar changes of the intraligand absorption band after the addition of a CT DNA solution, such as hypochromism up to 20%, as well as, in few cases, a red-shift (Table 2). The DNA-binding constants (K_b) of the complexes calculated by the Wolfe-Shimer equation [34] (Equation (1)) and plots $[\text{DNA}]/(\epsilon_A - \epsilon_f)$ versus $[\text{DNA}]$ (Figure S3) are similar to that of the corresponding free anthrapyrazoles (Table 2), except **ReL3** complex, which exhibited much higher K_b than **L3**, suggesting that its coordination to Re(I) results in a significant increase in the affinity for CT DNA. The K_b values suggest a strong binding of the anthrapyrazole ligands **L1**, **L2** and **L3** to CT DNA, which are similar to that of the classical intercalator EB ($=1.23 (\pm 0.07) \times 10^5 \text{ M}^{-1}$) [35]. The K_b value of complex **ReL3** ($=1.09 (\pm 0.15) \times 10^6 \text{ M}^{-1}$) is the highest DNA-binding constant among the herein examined compounds. However, the results obtained from the UV-vis spectroscopic titration studies (hypochromism) do not provide sufficient information to elucidate the type of interaction between the anthrapyrazoles and their rhenium complexes with DNA, and additional experiments are required to clarify the binding mode [24].

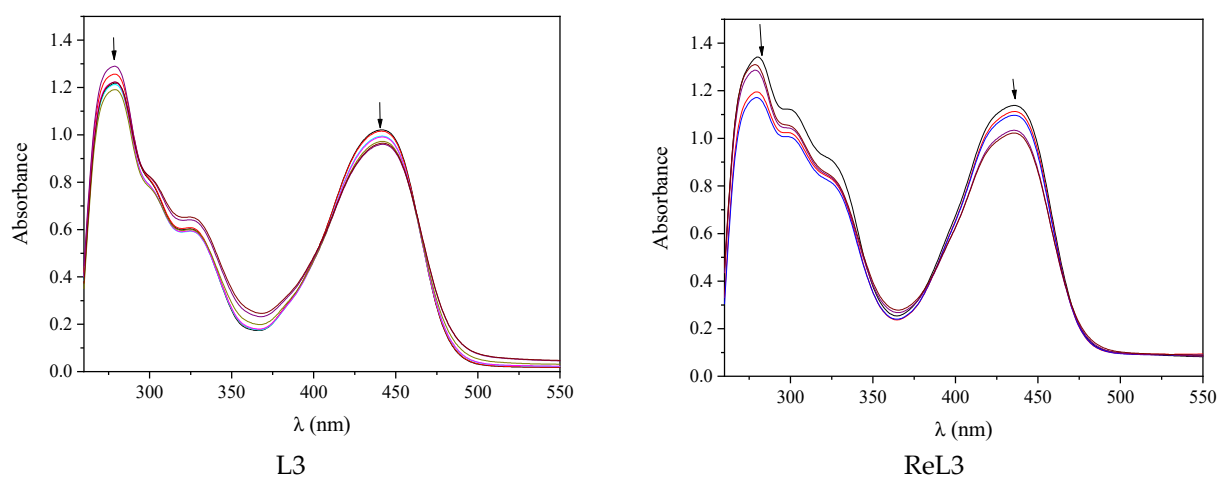


Figure 4. UV-vis spectra of DMSO solution ($1 \times 10^{-4} \text{ M}$) of **L3** and **ReL3** in the presence of increasing amounts of CT DNA. The arrows show the changes upon addition of CT DNA.

Table 2. Spectral features of the interaction of compounds **L1–L3** and **ReL1–ReL3** with CT DNA. UV band (λ_{max} , in nm), percentage of the observed hyper-/hypo-chromism ($\Delta A/A_0$, %), red-/blue-shift ($\Delta\lambda_{\text{max}}$, in nm) and DNA-binding constants (K_b , M^{-1}).

Compound	λ_{max} (nm) ($\Delta A/A_0$ (%) ^a , $\Delta\lambda_{\text{max}}$ (nm) ^b)	K_b (M^{-1})
L1	276 (−6 ^a , 0 ^b); 301 (sh) ^c (−5, 0); 323 (sh) (−7, 0); 439 (−7, 0)	$1.33 (\pm 0.01) \times 10^5$
L2	278 (−10, 0); 326 (sh) (−3.5, 0); 441 (−4, +2)	$7.74 (\pm 0.03) \times 10^4$
L3	277 (−7, +2); 325 (sh) (−7, 0); 441 (−6, 0)	$7.01 (\pm 0.01) \times 10^4$
ReL1	276 (−14, +3); 304 (−12, +2); 395 (−6.5, 0); 437 (sh) (−9, 0); 530 (−6, 0)	$1.24 (\pm 0.04) \times 10^5$
ReL2	278 (−20, +1); 300 (sh) (−10, 0); 435 (−5, +2)	$6.87 (\pm 0.09) \times 10^4$
ReL3	278 (−12, +2); 300 (sh) (−10, 0); 322 (sh) (−10, +2); 436 (−10, 0)	$1.09 (\pm 0.15) \times 10^6$

^a “+” denotes hyperchromism, “−” denotes hypochromism; ^b “+” denotes red-shift, “−” denotes blue-shift; ^c “sh” = shoulder.

Viscosity measurements were performed by the addition of increasing amounts of the anthrapyrazoles and their rhenium complexes on a CT DNA solution (10^{-4} M). The relative DNA viscosity (η/η_0) is sensitive to DNA length (L/L_0), and their relation is expressed by the equation $L/L_0 = (\eta/\eta_0)^{1/3}$ [36]. This study provides important information on the DNA-interaction mode of a tested compound by monitoring changes in DNA viscosity in

the presence of a compound. During intercalation, the DNA bases are separated to host the intercalator, which leads to the elongation of DNA and increased DNA viscosity. In the case of partial and/or non-classic intercalation (e.g., groove-binding or electrostatic interaction), the compounds do not enter in-between the DNA bases, and a bend or a kink in the DNA helix may occur, which does not significantly affect the DNA length, and the DNA viscosity remains practically unchanged or may even show a slight decrease. In the viscosity measurement, all the compounds resulted in a relative increase in the DNA viscosity (Figure 5). Such results indicate the insertion of the compounds between the DNA bases due to an intercalative interaction.

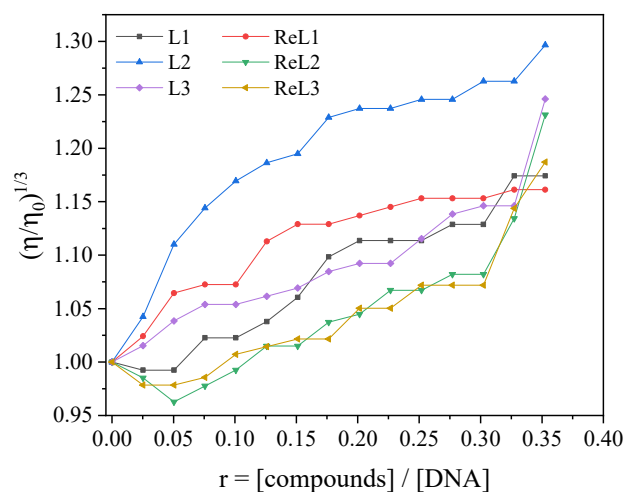


Figure 5. Relative viscosity $(\eta/\eta_0)^{1/3}$ of CT DNA (0.1 mM) in buffer solution (150 mM NaCl and 15 mM trisodium citrate at pH 7.0) in the presence of the compounds (anthrapyrazoles **L1–L3** and complexes **ReL1–ReL3**) at increasing amounts ($r = [\text{compound}]/[\text{DNA}]$).

The EB-displacing ability of the compounds by interaction with EB–DNA is considered to be useful in verifying the intercalation of a compound with DNA. EB is a typical intercalator, where the planar EB–phenanthridinium ring is inserted between adjacent base pairs on the double helix. The EB–DNA complex emits intense fluorescence at 592 nm (with $\lambda_{\text{excitation}} = 540$ nm), which may be quenched by a DNA-intercalating compound which competes with EB for DNA intercalation and is therefore used as a fluorescence dye [37].

The ligands and the rhenium complexes did not exhibit significant fluorescence in the presence of CT DNA and EB at 540 nm excitation; therefore, the complexes can be used as EB competitors in this study. The fluorescence emission spectra of pre-treated EB–CT DNA were obtained for $[\text{EB}] = 20 \mu\text{M}$, $[\text{DNA}] = 26 \mu\text{M}$ and for increasing amounts of the compounds (up to $r = 0.04$) (shown in Figures 6 and S4). The addition of increasing amounts of the ligands and rhenium complexes resulted in a substantial decrease in the intensity of the emission band of the DNA–EB complex at 592 nm (the fluorescence intensity in the highest competitor concentration was up to 43.5% of the initial EB–DNA fluorescence one, Table 3). Therefore, the tested compounds exhibited EB-displacing ability by competing with EB in binding to DNA (Figure 6B), proving thus, indirectly, their interaction with CT DNA via intercalation [38]. As seen from the Stern–Volmer plots of EB–DNA fluorescence studies in the presence of the competitors (Figure S5), the quenching of EB–DNA by the compounds is in agreement ($R = 0.99$) with the linear Stern–Volmer equation (Equation (2)), which proves the displacement of EB from EB–DNA by the compounds [34]. The obtained values of K_{SV} (Table 3) may show tight binding of the complexes to DNA. Since the fluorescence lifetime of EB–DNA (τ_0) is 23 ns [39], the K_{q} values were calculated with Equation (3). All quenching constants are higher than $10^{10} \text{ M}^{-1}\text{s}^{-1}$, indicating the presence of a static quenching mechanism which reveals the formation of a new adduct between the studied complexes and DNA, indirectly confirming intercalation as the most possible mode of interaction [37].

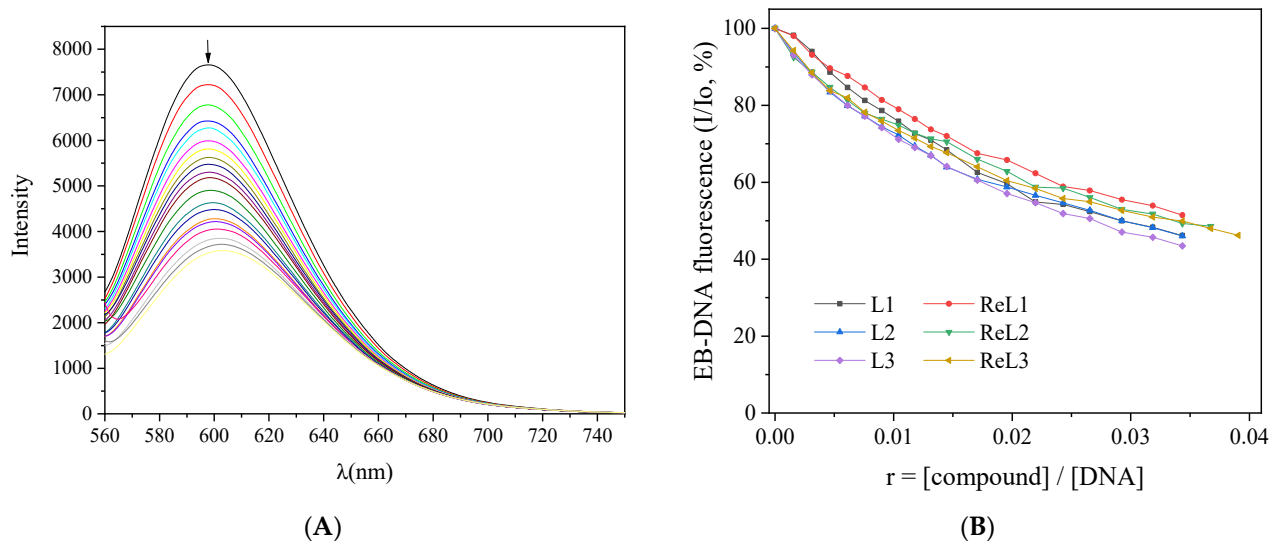


Figure 6. (A) Fluorescence emission spectra ($\lambda_{\text{excitation}} = 540 \text{ nm}$) of EB–DNA ($[\text{EB}] = 20 \mu\text{M}$, $[\text{DNA}] = 26 \mu\text{M}$) in buffer solution in increasing amounts of complex **ReL3** (up to the value of $r = 0.4$). The arrow shows the changes of intensity upon addition of **ReL3**. (B) Plot of EB–DNA relative fluorescence intensity at $\lambda_{\text{em}} = 592 \text{ nm}$ (I/I_0 , in %) (in buffer solution of 150 mM NaCl and 15 mM trisodium citrate at pH = 7.0) vs. r ($r = [\text{compound}]/[\text{DNA}]$) in the presence of the compounds (up to 46.1% of the initial EB–DNA fluorescence emission intensity for **L1**, 46.0% for **L2**, 43.5% for **L3**, 51.5% for **ReL1**, 48.6% for **ReL2**, and 46.1% for **ReL3**).

Table 3. Percentage of EB–DNA fluorescence quenching ($\Delta I/I_0$, %), the Stern–Volmer (K_{SV} , in M^{-1}) and EB–DNA quenching constants (K_{q} , in $\text{M}^{-1}\text{s}^{-1}$) for compounds **L1–L3** and **ReL1–ReL3**.

Compound	$\Delta I/I_0$ (%)	K_{sv} (M^{-1})	K_{q} ($\text{M}^{-1}\text{s}^{-1}$)
L1	53.9	$5.65 (\pm 0.09) \times 10^5$	$2.46 (\pm 0.04) \times 10^{13}$
L2	54.0	$5.27 (\pm 0.08) \times 10^5$	$2.29 (\pm 0.03) \times 10^{13}$
L3	56.5	$5.93 (\pm 0.04) \times 10^5$	$2.58 (\pm 0.02) \times 10^{13}$
ReL1	48.5	$4.47 (\pm 0.05) \times 10^5$	$1.94 (\pm 0.02) \times 10^{13}$
ReL2	51.4	$4.52 (\pm 0.07) \times 10^5$	$1.96 (\pm 0.03) \times 10^{13}$
ReL3	53.9	$4.60 (\pm 0.07) \times 10^5$	$2.00 (\pm 0.03) \times 10^{13}$

2.4. In Vitro Cell Studies

The cytotoxicity of the anthrapyrazole ligands **L1**, **L2** and **L3**, as well as that of the respective rhenium complexes **ReL1**, **ReL2** and **ReL3**, was assessed in vitro in colorectal adenocarcinoma cells CT26. The anthrapyrazole ligands **L1**, **L2**, **L3** and their rhenium complexes **ReL1**, **ReL2** and **ReL3** were incubated at 10^{-5} M concentration with the cells. Compounds **L2** and **ReL2** affected cell viability, exhibiting in average 82.55 ± 1.19 and $98.61 \pm 0.85\%$ decrease in cell proliferation and 83.92 ± 1.66 and $79.46 \pm 1.35\%$ cell death (Figure 7). The other four compounds tested (**L1**, **L3**, **ReL1**, **ReL3**) resulted in no significant cytotoxicity or cell death after incubation with the cells in this concentration. The most cytotoxic compounds **L2** and **ReL2** were tested at lower concentrations up to 10^{-7} M , and the IC_{50} was calculated to be $0.36 \mu\text{M}$ for **L2** and $0.64 \mu\text{M}$ for **ReL2** (Figure S6). The cytotoxicity of these compounds is in the same range as for other standard cytotoxic agents from the literature, such as doxorubicin and cisplatin [40,41]. The fact that ligands **L1** and **L3** are not active in this concentration range is clearly attributed to their structure. By comparison to anthrapyrazoles and similar compounds in the literature, it is evident that the pyrazole nitrogen substitution is important for its cytotoxicity [24,42–44], while both losoxantrone and mitoxantrone clinical agents contain $-\text{NCH}_2\text{CH}_2\text{NHCH}_2\text{CH}_2\text{OH}$ moieties.

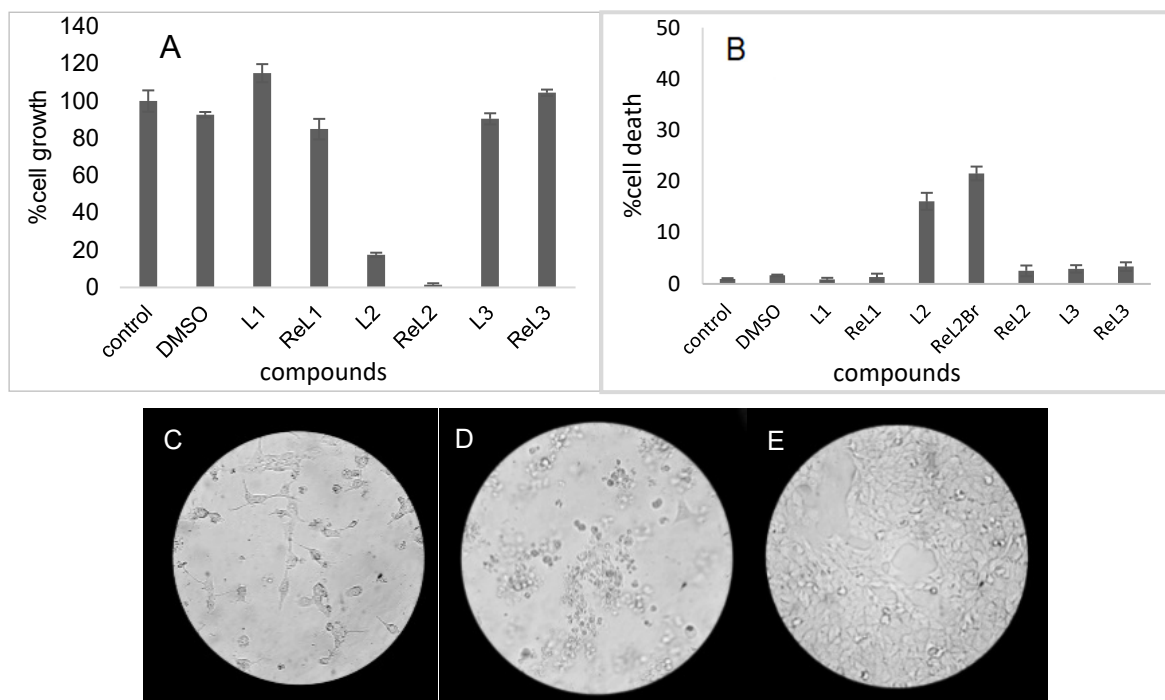


Figure 7. Assessment of cell growth (A) and the proportion of dead cells (B) in cultures of CT 26 incubated with 10⁻⁵ M of each compound. The morphology of CT 26 treated with 10⁻⁵ M of either L2 (D) and ReL2 (C) along with the untreated control culture (E) is shown.

2.5. Radiotracer Studies

Technetium-99m (^{99m}Tc) is a γ -emitting radionuclide with excellent physical properties ($t_{1/2}$: 6.01 h, 0.142 MeV). In addition, its low-cost commercial availability from ⁹⁹Mo/^{99m}Tc generators makes it an efficient choice in nuclear medicine for SPECT imaging. Technetium and rhenium are considered congener metals, and usually, they form isostructural complexes with similar biological properties [45]. The first in vivo evaluation of the potential ability of **ReL2** to be distributed to the tumor was conducted by preparing an analogous γ -emitting radiotracer, *fac*-[^{99m}Tc][Tc(CO)₃(**L2**)(H₂O)]⁺ (^{99m}Tc**L2**). Furthermore, in an effort to explain the low biological activity of the complex **ReL3**, we prepared the analogous radiotracer ^{99m}Tc**L3**.

^{99m}Tc**L2** and ^{99m}Tc**L3** were synthesized by reaction of the aqua ion *fac*-[^{99m}Tc][Tc(CO)₃(H₂O)₃]⁺ with 10⁻³ M of the ligand **L2** or **L3** for 30 min at 55–65 °C, with high radiochemical purity of >95%. ^{99m}Tc**L2**, $t_R = 19.2$ min was identified by comparative RP-HPLC studies, using complexes [Re(CO)₃(**L2**)Br] (**ReL2**), $t_R = 21.1/21.3$ min and [Re(CO)₃(**L2**)(MeOH)]⁺ (**ReL2'**) (which was formed from **ReL2** by precipitation of bromide with silver salts) $t_R = 19.1$ min as references (Figure S7). ^{99m}Tc**L3**, $t_R = 21.3$ min and **ReL3**, $t_R = 21.4$ min were identified. The lipophilicity value of the HPLC-purified ^{99m}Tc**L2** was found to be 2.45 ± 0.06 , and that of ^{99m}Tc**L3** was found to be 2.27 ± 0.12 , which indicates that the complexes could penetrate cell membranes and be distributed across various tissues and organs. The stability of ^{99m}Tc**L2** was tested after incubation with 1 mM histidine and rat plasma, and the percentage of intact tracer was found to be 95% at 4 h in histidine and 82% at 4 h in rat plasma, where it exhibited 54% protein binding. Respectively, ^{99m}Tc**L3** was 93% stable in histidine and 95% stable in rat plasma (with low protein binding of 16.4%) at 4 h.

The cellular uptake of tracer ^{99m}Tc**L2** and ^{99m}Tc**L3** was performed in CT26 cells over 240 min. ^{99m}Tc**L2** exhibited a time-dependent increase in cell uptake reaching $5.42 \pm 0.19\%$ cells at 240 min after incubation. ^{99m}Tc**L3** exhibited low cell uptake. In detail, Table 4 shows the results obtained:

Table 4. Percentage (%) of $^{99m}\text{TcL2}$ and $^{99m}\text{TcL3}$ uptake in CT26 cells.

	15 min	60 min	120 min	240 min
$^{99m}\text{TcL2}$	$1.29 \pm 0.09\%$	$2.48 \pm 0.25\%$	$3.94 \pm 0.68\%$	$5.42 \pm 0.19\%$
$^{99m}\text{TcL3}$	$0.49 \pm 0.06\%$	$0.53 \pm 0.04\%$	$0.55 \pm 0.08\%$	$0.75 \pm 0.11\%$

Biodistribution studies were performed in CT26 tumor-bearing mice at time points of 30 and 120 min post intravenous injection of $^{99m}\text{TcL2}$ (Table 5). The radiotracer $^{99m}\text{TcL2}$ exhibited hepatobiliary and renal elimination, while the percentage of radioactivity in the blood was $4.16 \pm 1.31\%$ ID/g at 120 min. The tumor uptake of $^{99m}\text{TcL2}$ was 2.42 ± 0.04 and $3.10 \pm 1.21\%$ ID/g at 30 and 120 min, respectively, which shows retention of the tracer in the tumor up to 2 h.

Table 5. Distribution of $^{99m}\text{TcL2}$ in CT26 tumor-bearing mice (%ID/g).

Organ	%ID/g	
	30 min	120 min
Blood	6.48 ± 2.02	4.16 ± 1.31
Tumor (CT26)	2.42 ± 0.04	3.10 ± 1.21
Heart	8.91 ± 3.77	5.90 ± 1.16
Liver	29.49 ± 9.43	24.51 ± 7.12
Lungs	15.36 ± 6.43	7.73 ± 2.29
Muscle	2.17 ± 0.25	2.20 ± 0.51
Kidneys	22.09 ± 8.91	17.04 ± 3.53
Spleen	6.78 ± 1.33	3.87 ± 0.87
Intestine	11.38 ± 3.43	19.84 ± 8.10
Stomach	8.58 ± 6.60	14.26 ± 7.53

3. Materials and Methods

3.1. General

All chemicals were reagent-grade. For the chromatographic purifications, Silica gel 60 (0.040–0.063 mm) from Merck (Darmstadt, Germany) was used. The precursors $[\text{Re}(\text{CO})_5\text{Br}]$ and $[\text{Re}(\text{CO})_5(\text{OTf})]$ were prepared according to literature procedures [46,47]. For labeling with ^{99m}Tc , a vial containing 5.5 mg of NaBH_4 , 4 mg of Na_2CO_3 , and 15 mg of Na-K tartrate was purged with CO gas prior to addition of $\text{Na}^{99m}\text{TcO}_4$, as described in the literature [48]. Solvents used for high-performance liquid chromatography (HPLC) were HPLC-grade, and solvents used for mass spectroscopy (MS) were MS-grade. To prepare the HPLC mobile phase, the solvents were filtered through membrane filters (0.22 μm , Millipore, Milford, MA, USA) and degassed. UV-visible (UV-vis) spectra were recorded on a Hitachi U-2001 (Hitachi, Tokyo, Japan) dual beam spectrophotometer. C, H and N elemental analysis were performed on a Perkin-Elmer 240B elemental analyzer (Perkin Elmer, Waltham, MA, USA). Fluorescence spectra were recorded in solution on a Hitachi F-7000 (Hitachi, Tokyo, Japan) fluorescence spectrophotometer. Viscosity experiments were carried out using an ALPHA L Fungilab (Barcelona, Spain) rotational viscometer equipped with an 18 mL LCP spindle and the measurements were performed at 100 rpm. The ESI-HRMS spectra were recorded on an Agilent Q-TOF Mass Spectrometer, G6540B model with Dual AJS ESI-MS (Santa Clara, CA, USA). IR spectra were recorded on a Spectrum BX spectrophotometer (Perkin Elmer, Waltham, MA, USA) in the region 4000–500 cm^{-1} . NMR spectra were recorded on a DD2 500 MHz spectrometer (Agilent, Santa Clara, CA, USA), respectively. The HPLC system used comprised an Agilent HP 1100 series pump (HP, Waldbronn, Germany), connected to a Gabi gamma detector (Raytest, Straubenhardt, Germany) and an HP 1100 multiple wavelength detector. RP-HPLC analyses of the rhenium and technetium-99m complexes were performed using an Agilent Eclipse XDB C18 column (25 cm \times 4.6 mm, 5 μm) by applying a binary gradient method of Solvent A: H_2O —0.1% TFA and Solvent B: Methanol.

The flow rate was set at 1 mL/min, and the composition was as follows: (min, A%, B%); (0, 100, 0); (15, 25, 75); (20, 5, 95); (25, 5, 95); (27, 100, 0); (30, 100, 0).

Calf thymus (CT) DNA (Merck, Darmstadt, Germany) was diluted in buffer (consisting of 15 mM trisodium citrate and 150 mM NaCl at pH 7.0) followed by continuous stirring for three days for the preparation of the DNA stock solution, which was kept at 4 °C for up to a week. The ratio of UV absorbance of the CT DNA stock solution at 260 and 280 nm (A_{260}/A_{280}) was measured to be 1.85, indicating that it was free of protein contamination [49]. The DNA concentration was determined by the UV absorbance at 260 nm after 1:20 dilution using $\epsilon = 6600 \text{ M}^{-1}\text{cm}^{-1}$ [50].

CAUTION! $^{99\text{m}}\text{Tc}$ is a gamma (γ)-emitter with nuclear properties of $t_{1/2} = 6 \text{ h}$ and γ -energy, 140 keV. Its handling was performed according to Greek legislation and the EU regulations (2013/59/Euratom). $^{99\text{m}}\text{Tc}$ was obtained as sodium pertechnetate in sterile saline from a commercial $^{99}\text{Mo}/^{99\text{m}}\text{Tc}$ generator (AHEPA General Hospital, Thessaloniki, Greece).

3.2. Syntheses

1-Tosyl-8-methoxy-9,10-anthraquinone (2): 1,8-dihydroxy-anthraquinone (240 mg, 1 mmol) and potassium carbonate (138 mg, 1 mmol) were dissolved in dry acetone (50 mL). To this solution, dimethyl sulfate (130 μL , 1.3 mmol) was added dropwise, and the mixture was refluxed for 24 h. Then, sulfuric acid 0.1 M (5 mL) was added, and the mixture was concentrated to dryness under vacuum, followed by the addition of distilled water (300 mL). The precipitate that contained 1-hydroxy-8-methoxy-9,10-anthraquinone was isolated through filtration under vacuum, and the crude product was purified by silica gel (15 g) column chromatography with petroleum ether:ethyl acetate, 90:10–80:20, to afford a yellow solid. Yield: 120 mg, 47.2%. R_f : (SiO₂, petroleum ether:ethyl acetate, 9:1) 0.62. ^1H NMR (500 MHz, CDCl₃, ppm) δ : 12.99 (s, 1H), 7.97 (d, $J = 7.7 \text{ Hz}$, 1H), 7.79–7.72 (m, 2H), 7.62 (t, $J = 7.9 \text{ Hz}$, 1H), 7.37 (d, $J = 8.5 \text{ Hz}$, 1H), 7.29 (d, $J = 8.4 \text{ Hz}$, 1H), 4.08 (s, 3H). Then, 1-hydroxy-8-methoxy-9,10-anthraquinone (3 g, 11.8 mmol), potassium carbonate (1.63 g, 11.8 mmol) and p-toluenesulfonyl chloride (4.6 g, 24 mmol) were mixed in dry acetone (300 mL). The mixture was refluxed for 72 h. A brown solid formed, which was filtered under vacuum and dried. Yield: 2.2 g, 45.7%. R_f : (SiO₂, petroleum ether:ethyl acetate, 7:3) 0.5. m.p. 190–193 °C [24]. ^1H NMR (500 MHz, CDCl₃, ppm) δ : 8.17 (dd, $J = 7.7$, 1.2 Hz, 1H), 7.87 (d, $J = 8.3 \text{ Hz}$, 2H), 7.83 (dd, $J = 7.6$, 0.7 Hz, 1H), 7.66 (t, $J = 8.0 \text{ Hz}$, 2H), 7.57 (dd, $J = 8.1$, 1.1 Hz, 1H), 7.30 (t, $J = 8.9 \text{ Hz}$, 3H), 4.02 (s, 3H), 2.38 (s, 3H). ^{13}C NMR (126 MHz, CDCl₃, ppm) δ : 197.22, 187.33, 182.69, 180.65, 159.56, 146.91, 145.36, 134.65, 134.59, 134.47, 133.29, 132.40, 129.98, 129.59, 129.16, 128.91, 125.76, 123.23, 119.17, 118.26, 56.65, 21.68. ESI-HRMS (m/z): Calc. for $\text{M} = \text{C}_{22}\text{H}_{16}\text{SO}_6$: 409.0740 [$\text{M} + \text{H}$]⁺, 431.0560 [$\text{M} + \text{Na}$]⁺; Found: 409.0726 [$\text{M} + \text{H}$]⁺, 431.0566 [$\text{M} + \text{Na}$]⁺.

2-(2-Hydroxyethyl)-10-methoxy-anthra [1,9-cd]pyrazol-6(2H)-one (3): Compound 2 (200 mg, 0.49 mmol) and 2-hydroxyethylhydrazine (168 μL , 2.47 mmol) were dissolved in anhydrous N,N-dimethylformamide (DMF) (10 mL). The mixture was heated at 130 °C, under nitrogen, for 4 h. The reaction mixture was partitioned between ethyl acetate (50 mL) and water (50 mL), and the organic phase was collected and concentrated to dryness. The crude product was purified by silica gel column chromatography (60 g) with ethyl acetate:petroleum ether, starting with 70:30 up to 90:10, to afford a yellow solid. Yield: 36 mg, 25%. R_f : (SiO₂, ethyl acetate:petroleum ether, 9:1) 0.01. m.p. 245–248 °C [8]. ^1H NMR (500 MHz, CDCl₃, ppm) δ : 8.11 (d, $J = 7.8 \text{ Hz}$, 1H), 8.03 (d, $J = 7.1 \text{ Hz}$, 1H), 7.76 (d, $J = 8.2 \text{ Hz}$, 1H), 7.66 (t, $J = 7.7 \text{ Hz}$, 1H), 7.51 (t, $J = 8.0 \text{ Hz}$, 1H), 7.28 (d, $J = 5.4 \text{ Hz}$, 1H), 4.68 (t, $J = 4.8 \text{ Hz}$, 2H), 4.27 (t, $J = 4.8 \text{ Hz}$, 2H), 4.12 (s, 3H). ^{13}C NMR (126 MHz, d₆-DMSO, ppm) δ : 183.01, 156.40, 139.46, 136.47, 134.31, 129.09, 128.28, 125.28, 123.38, 121.07, 120.97, 120.44, 117.40, 116.83, 60.92, 56.62, 52.71. ESI-HRMS (m/z): Calc. for $\text{M} = \text{C}_{17}\text{H}_{14}\text{N}_2\text{O}_3$: 295.1077 [$\text{M} + \text{H}$]⁺, 317.0897 [$\text{M} + \text{Na}$]⁺; Found: 295.1083 [$\text{M} + \text{H}$]⁺, 317.0897 [$\text{M} + \text{Na}$]⁺.

2-(2-Hydroxyethyl)-10-hydroxy-anthra [1,9-cd]pyrazol-6(2H)-one (L1): Compound 3 (260 mg, 0.88 mmol) was dissolved in anhydrous dichloromethane (50 mL) and was stirred at $-10 \text{ }^\circ\text{C}$. To this solution, boron tribromide 1 M (5.85 mL, 5.2 mmol) in dichloromethane was added

dropwise, under nitrogen, for 1 h. The mixture was then stirred at rt (25 °C) for 24 h. Then, distilled water was added (50 mL) dropwise at −10 °C, for 1 h. The reaction mixture was partitioned between aqueous NaHCO₃ 1 M (50 mL) and dichloromethane (50 mL) and the organic phase was collected and concentrated to dryness. The crude product was washed three times with dichloromethane (3 × 10 mL), and a brown solid formed, which was filtered and dried. Yield: 160 mg, 65%. RP-HPLC retention time (t_R): 18.2 min. R_f: (SiO₂, ethyl acetate) 0.38. m.p. 190–193 °C. IR (cm^{−1}, KBr): 3406, 3076, 2934, 1636, 1593, 1459, 1396, 1351, 1282, 1262. ¹H NMR (500 MHz, d₆-DMSO, ppm) δ: 9.87 (s, 1H), 8.11 (d, J = 8.2 Hz, 1H), 7.94 (d, J = 7.1 Hz, 1H), 7.85 (d, J = 7.6 Hz, 1H), 7.75 (t, J = 7.6 Hz, 1H), 7.44 (t, J = 7.9 Hz, 1H), 7.35 (d, J = 7.9 Hz, 1H), 4.97 (br, 1H), 4.66 (t, J = 5.3 Hz, 2H), 3.92 (t, J = 5.3 Hz, 2H). ¹³C NMR (126 MHz, d₆-DMSO, ppm) δ: 183.21, 154.43, 139.40, 137.17, 134.26, 129.19, 128.71, 125.56, 122.95, 121.11, 120.49, 120.31, 118.67, 117.37, 60.87, 52.68. ESI-HRMS (m/z): Calc. for M=C₁₆H₁₂N₂O₃: 279.0775 [M−H][−], 248.0580 [M−CH₃OH][−]; Found: 279.0658 [M−H][−], 248.0489 [M−CH₃OH][−].

2-(2-Methylsulfonylethyl)-10-methoxy-anthra [1,9-cd]pyrazol-6(2H)-one (4): Compound **3** (250 mg, 0.85 mmol) and triethylamine (840 μL, 5.9 mmol) were dissolved in anhydrous dichloromethane (50 mL). To this solution, methanesulfonyl chloride (490 μL, 5.9 mmol) in dry dichloromethane (5 mL) was added dropwise at −10 °C, under nitrogen, for 30 min. The mixture was stirred at 25 °C, under nitrogen, for 4 h. The reaction mixture was concentrated to dryness under vacuum and was extracted between distilled water (50 mL) and ethyl acetate (50 mL). The organic phase was concentrated to dryness under vacuum, to afford a yellow solid. Yield: 317 mg, 85%. R_f: (SiO₂, ethyl acetate) 0.26. m.p. 155–158 °C. ¹H NMR (500 MHz, CDCl₃, ppm) δ: 8.14 (d, J = 7.8 Hz, 1H), 8.08 (d, J = 7.1 Hz, 1H), 7.81 (d, J = 8.2 Hz, 1H), 7.70 (t, J = 7.7 Hz, 1H), 7.53 (t, J = 8.0 Hz, 1H), 7.32 (d, J = 8.2 Hz, 1H), 4.92 (t, J = 5.1 Hz, 2H), 4.81 (t, J = 5.1 Hz, 2H), 4.14 (s, 3H), 2.80 (s, 3H). ¹³C NMR (126 MHz, CDCl₃, ppm) δ (ppm): 182.93, 156.40, 138.95, 138.01, 134.79, 129.80, 129.51, 126.26, 123.38, 121.77, 121.46, 119.48, 115.87, 115.15, 68.16, 56.45, 48.92, 37.42. ESI-HRMS (m/z): Calc. for M=C₁₈H₁₆N₂SO₅: 373.0853 [M + H]⁺, 395.0672 [M + Na]⁺. Found: 373.0850 [M + H]⁺, 395.0666 [M + Na]⁺.

2-(2-Picolylaminoethyl)-10-methoxy-anthra [1,9-cd]pyrazol-6(2H)-one (L2): Compound **4** (290 mg, 0.75 mmol) and 2-(aminomethyl)pyridine (1.48 mL, 15 mmol) were dissolved in anhydrous methanol (70 mL), and the mixture was refluxed for 24 h. The reaction mixture was concentrated to dryness under vacuum and extracted in ethyl acetate–water (3 × 50 mL). The organic phase was concentrated to dryness under vacuum. The crude product was purified by silica gel (20 g) column chromatography with dichloromethane:methanol, 95:5, to afford a brown oil. Yield: 110 mg, 39%. t_R: 16.4 min. R_f: (SiO₂, dichloromethane:methanol, 9:1) 0.18. IR (cm^{−1}, KBr): 3451, 1639, 1578, 1455, 1281, 1270. ¹H NMR (500 MHz, CDCl₃, ppm) δ: 8.48 (d, J = 4.6 Hz, 1H), 8.12 (d, J = 7.9 Hz, 1H), 8.04 (d, J = 7.2 Hz, 1H), 7.76 (d, J = 8.2 Hz, 1H), 7.63 (t, J = 7.7 Hz, 1H), 7.58 (t, J = 7.6 Hz, 1H), 7.48 (td, J = 8.1, 1.1 Hz, 1H), 7.28 (d, J = 8.2 Hz, 1H), 7.25 (d, J = 8.1 Hz, 1H), 7.12 (t, J = 6.2 Hz, 1H), 4.74 (t, J = 6.0 Hz, 2H), 4.09 (s, 3H), 3.98 (s, 2H), 3.34 (t, J = 5.8 Hz, 2H), 2.37 (s, 1H). ¹³C NMR (126 MHz, CDCl₃, ppm) δ: 183.65, 159.02, 156.30, 149.24, 138.76, 137.78, 136.48, 134.81, 128.62, 128.06, 126.16, 124.00, 122.13, 122.06, 121.67, 121.06, 120.62, 115.71, 114.97, 56.46, 54.72, 49.86, 48.98. ESI-HRMS (m/z): Calc. for C₂₃H₂₀N₄O₂: 385.1659 [M + H]⁺, 407.1478 [M + Na]⁺. Found: 385.1640 [M + H]⁺, 407.1466 [M + Na]⁺.

Ethyl 2-((2-(10-methoxy-6-oxodibenzo[cd,g]indazol-2(6H)-yl)ethyl)(pyridin-2-ylmethyl)amino)acetate (**L3**): First, ethyl 2-((pyridin-2-ylmethyl)amino)acetate was prepared by a modification of the procedure published elsewhere [51]. Specifically, ethyl bromoacetate (1.67 g, 10 mmol), 2-(aminomethyl)pyridine (1.48 mL, 15 mmol) and potassium carbonate (4 g, 30 mmol) were dissolved in dry acetonitrile (200 mL). The mixture was refluxed for 1 h. The reaction mixture was filtered and concentrated to dryness under vacuum. The crude product was purified by silica gel (60 g) flash chromatography with dichloromethane:methanol: aqueous ammonia solution 10%, 90:10:0.1, to afford a brown oil. Yield: 1.3 g, 67%. R_f: (SiO₂, dichloromethane:methanol: aqueous ammonia solution

10%, 9:1:0.1) 0.69. ^1H NMR (500 MHz, CDCl_3) δ (ppm): 8.56 (d, $J = 4.2$ Hz, 1H), 7.65 (td, $J = 7.7, 1.8$ Hz, 1H), 7.34 (t, $J = 7.8$ Hz, 1H), 7.19–7.14 (m, 1H), 4.18 (dq, $J = 14.6, 7.1$ Hz, 2H), 3.96 (s, 2H), 3.48 (s, 2H), 1.27 (t, $J = 7.1$ Hz, 3H).

Consequently, compound **4** (390 mg, 1.01 mmol) and ethyl 2-((pyridin-2-ylmethyl)amino)acetate (1.3 g, 6.7 mmol) were dissolved in dry methanol (100 mL). The mixture was refluxed, under nitrogen, for 72 h. The reaction mixture was concentrated to dryness under vacuum and extracted in ethyl acetate–water (3×50 mL). The organic phase was concentrated to dryness under vacuum. The crude product was purified by silica gel (60 g) column chromatography with dichloromethane:methanol, 98:2, to afford a brown oil. Yield: 160 mg, 34%. t_{R} : 17.3 min. R_{f} : (SiO_2 , dichloromethane:methanol, 9:1) 0.55. IR (cm^{-1} , KBr): 3451, 2936, 1737, 1647, 1455, 1290, 1270. ^1H NMR (500 MHz, CDCl_3 , ppm) δ : 8.44 (d, $J = 4.8$ Hz, 1H), 8.12 (d, $J = 7.8$ Hz, 1H), 8.03 (d, $J = 7.1$ Hz, 1H), 7.69 (dd, $J = 8.2, 2.0$ Hz, 1H), 7.59 (t, $J = 7.7$ Hz, 1H), 7.48 (t, $J = 8.0$ Hz, 1H), 7.36 (m, 1H), 7.28 (d, $J = 8.2$ Hz, 1H), 7.08 (d, $J = 7.8$ Hz, 1H), 7.03 (m, 1H), 4.66 (t, $J = 6.4$ Hz, 2H), 4.13 (dd, $J = 14.0, 6.8$ Hz, 2H), 4.10 (s, 3H), 4.00 (d, $J = 2.3$ Hz, 2H), 3.51 (d, $J = 2.7$ Hz, 2H), 3.39 (t, $J = 6.4$ Hz, 2H), 1.22 (t, $J = 7.1$ Hz, 3H). ^{13}C NMR (126 MHz, d_6 -DMSO, ppm) δ : 183.71, 171.18, 158.69, 156.22, 148.53, 138.63, 137.42, 136.65, 134.75, 128.55, 127.88, 126.01, 123.97, 123.06, 122.14, 121.65, 121.12, 120.52, 115.67, 115.26, 60.57, 56.48, 55.56, 53.92, 51.53, 48.81, 14.22. ESI-HRMS (m/z): Calc. for $\text{M}=\text{C}_{27}\text{H}_{26}\text{N}_4\text{O}_4$: 471.2027 $[\text{M} + \text{H}]^+$, 493.1846 $[\text{M} + \text{Na}]^+$. Found: 471.2032 $[\text{M} + \text{H}]^+$, 493.1846 $[\text{M} + \text{Na}]^+$.

Synthesis of ReL1: $[\text{Re}(\text{CO})_5\text{Br}]$ (81.2 mg, 0.20 mmol) and **L1** (56 mg, 0.20 mmol) were dissolved in methanol (40 mL), and the mixture was refluxed for 24 h. The mixture was concentrated to dryness under vacuum, followed by the addition of distilled water (10 mL). After 24 h, a precipitate was formed at room temperature and was isolated through filtration under vacuum. The crude product was purified by silica gel (60 g) column chromatography with dichloromethane:methanol, 98:2–90:10, to afford a red solid. Yield: 45 mg, 38.5%. t_{R} : 18.8 min. R_{f} : (SiO_2 , dichloromethane:methanol, 9:1) 0.67. m.p. 249–252 °C. Calc. for $\text{C}_{20}\text{H}_{15}\text{N}_2\text{O}_7\text{Re}$: C, 41.31; H, 2.60; N, 4.82; Found: C 41.55; H 2.91; N 4.71. IR (cm^{-1} , KBr): 3432 (O-H), 2936 (C-H), 2025 (CO), 1930 (CO), 1900 (CO), 1636 (C=O), 1566 (C=N), 1459 (arom. C-C, C-N), 1282 (C-O). ^1H NMR (500 MHz, d_6 -DMSO, ppm) δ : 8.10 (d, $J = 8.3$ Hz, 1H), 7.95 (d, $J = 7.0$ Hz, 1H), 7.87 (dd, $J = 8.2, 7.2$ Hz, 1H), 7.54 (dd, $J = 7.5, 1.0$ Hz, 1H), 7.40 (t, $J = 8.2, 7.6$ Hz, 1H), 7.18 (dd, $J = 7.3, 1.0$ Hz, 1H), 5.07 (t, $J = 5.4$ Hz, 1H), 4.89–4.84 (m, 1H), 4.05–3.87 (m, 2H), 5.03 (t, $J = 5.3$ Hz, 1H), 4.90–4.85 (m, 2H), 4.03–3.96 (m, 1H), 3.96–3.89 (m, 1H). ^{13}C NMR (126 MHz, d_6 -DMSO, ppm) δ : 197.88, 197.36, 196.86, 182.96, 160.30, 140.80, 138.65, 133.86, 131.39, 131.13, 126.59, 126.39, 121.40, 120.48, 117.96, 116.92, 116.49, 60.30, 52.36. ESI-HRMS (m/z): Calc. for $\text{M} = \text{C}_{20}\text{H}_{15}\text{N}_2\text{O}_7\text{Re}$: 579.0318 (60%), 581.0311 (100%) $[\text{M}-\text{H}]^-$. Found: 579.0101 (60%), 581.0139 (100%) $[\text{M}-\text{H}]^-$.

Synthesis of ReL2: $[\text{Re}(\text{CO})_5\text{Br}]$ (65 mg, 0.16 mmol) and **L2** (60 mg, 0.16 mmol) were dissolved in methanol (35 mL), and the mixture was refluxed for 3 h. The yellow solid formed was filtered under vacuum, recrystallized from methanol–water and dried. Yield: 55 mg, 47%. t_{R} : 21.1 min, 21.3 min. R_{f} : (SiO_2 , dichloromethane:methanol, 9:1) 0.89. m.p. 336–339 °C. Calc. for $\text{C}_{26}\text{H}_{20}\text{N}_4\text{O}_5\text{ReBr}$: C, 42.51; H, 2.74; N, 7.63; Found: C 42.82; H 2.99; N 7.68. IR (cm^{-1} , KBr): 3448, 3168 (N-H), 2935 (C-H), 2021 (CO), 1909 (CO), 1867 (CO), 1654 (C=O), 1636 (C=N), 1438 (arom. C-C, C-N), 1284 (C-O), 1267 (C-O). ^1H NMR (500 MHz, d_6 -DMSO, ppm) *Major*/ δ : 8.78 (d, $J = 5.1$ Hz, 1H), 8.17 (d, $J = 8.2$ Hz, 1H), 8.10 (td, $J = 7.8, 1.5$ Hz, 1H), 7.96 (dd, $J = 7.1, 1.7$ Hz, 1H), 7.92 (dd, $J = 7.8, 1.0$ Hz, 1H), 7.79 (m, 2H), 7.56 (t, $J = 7.7$ Hz, 1H), 7.55 (t, $J = 8.0$ Hz, 1H), 7.45 (d, $J = 7.6$ Hz, 1H), 5.64 (s, 1H), 5.12 (dd, $J = 15.9, 5.2$ Hz, 1H), 4.94 (dd, $J = 12.2, 5.8$ Hz, 2H), 4.43 (dd, $J = 15.9, 8.8$ Hz, 1H), 3.80 (s, 3H), 3.74 (m, 2H); *minor*/ δ : 8.79 (d, $J = 5.1$ Hz), 8.18 (d, $J = 8.2$ Hz, 1H), 8.06 (td, $J = 7.8, 1.5$ Hz), 7.96 (dd, $J = 7.1, 1.7$ Hz, 1H), 7.93 (dd, $J = 7.8, 1.0$ Hz, 1H), 7.79 (t, $J = 7.7$ Hz, 1H), 7.68 (d, $J = 7.9$ Hz), 7.55 (t, $J = 8.0$ Hz, 1H), 7.49 (d, $J = 7.6$ Hz, 1H), 7.48 (m, 1H), 6.73 (s, 1H), 4.97–4.83 (m, 2H), 4.72 (dd, $J = 15.6, 5.3$ Hz, 1H), 4.60 (dd, $J = 15.7, 8.8$ Hz), 3.91 (s), 3.74 (m, 2H). ^{13}C NMR (126 MHz, d_6 -DMSO, ppm) *Major*/ δ : 197.87, 196.58, 192.21, 182.97, 160.69, 156.57, 153.12, 140.38, 138.80, 137.46, 134.33, 129.57, 128.99, 125.90, 125.53, 123.52, 123.26,

120.94, 120.45, 116.90, 109.98, 58.64, 57.44, 56.62, 47.26; *minor*/δ: 197.87, 196.58, 192.21, 182.97, 161.80, 156.51, 153.05, 140.34, 138.92, 137.26, 134.34, 129.63, 128.91, 125.79, 125.54, 123.31, 123.26, 121.05, 120.62, 117.06, 116.77, 58.80, 57.68, 56.69, 47.26. ESI-HRMS (*m/z*): Calc. for $M=C_{26}H_{20}N_4O_5ReBr$: 653.0946 (60%), 655.0783 (100%) $[M-Br]^+$, 731.0995 (60%), 733.1125 (100%) $[M-Br + DMSO]^+$. Found: 653.0747 (60%), 655.0960 (100%) $[M-Br]^+$, 731.1110 (60%), 733.1138 (100%) $[M-Br + DMSO]^+$.

Synthesis of ReL3: $[Re(CO)_5(OTf)]$ (22 mg, 0.05 mmol) was dissolved in methanol (7 mL), and the mixture was refluxed for 1 h for the formation of $[Re(CO)_3(MeOH)_3]^+$. **L3** (24 mg, 0.05 mmol) was added, and the mixture was refluxed for 24 h. The reaction mixture was concentrated to ~3 mL, and after cooling, a yellow solid was formed, which was filtered under vacuum and dried. Yield: 21 mg, 60%. t_R : 21.4 min. R_f : (SiO₂, dichloromethane:methanol, 9:1) 0.78. m.p. 327–330 °C. Calc. for $C_{28}H_{21}N_4O_7Re$: C, 47.25; H, 2.97; N, 7.87; Found: C, 47.48; H 3.15; N 7.56. IR (cm⁻¹, KBr): 3449, 2941 (C-H), 2023 (CO), 1912 (CO), 1870 (CO), 1651 (C=O), 1457 (arom. C-C, C-N), 1296 (C-O), 1267 (C-O). ¹H NMR (500 MHz, d₆-DMSO, ppm) δ: 8.78 (d, *J* = 5.4 Hz, 1H), 8.30 (d, *J* = 8.2 Hz, 1H), 8.16 (t, *J* = 7.7 Hz, 1H), 7.98 (d, *J* = 7.1 Hz, 1H), 7.94 (d, *J* = 7.7 Hz, 1H), 7.81 (t, *J* = 7.8 Hz, 1H), 7.72 (d, *J* = 7.9 Hz, 1H), 7.59 (t, *J* = 6.6 Hz, 1H), 7.56 (t, *J* = 7.9 Hz, 1H), 7.51 (d, *J* = 8.1 Hz, 1H), 5.13–5.03 (m, 2H), 5.04 (d, *J* = 15.5 Hz, 1H), 4.85 (d, *J* = 15.7 Hz, 1H), 4.28 (dt, *J* = 13.8, 7.0 Hz, 1H), 4.16 (dt, *J* = 13.3, 6.7 Hz, 1H), 4.03 (d, *J* = 16.6 Hz, 1H), 4.02 (s, 3H), 3.59 (d, *J* = 16.6 Hz, 1H). ¹³C NMR (126 MHz, d₆-DMSO, ppm) δ: 198.00, 197.34, 182.96, 178.92, 159.68, 156.54, 152.55, 141.18, 138.80, 137.28, 134.42, 129.62, 128.93, 126.45, 125.56, 124.27, 123.60, 121.16, 120.96, 120.58, 117.20, 117.16, 67.99, 67.45, 61.32, 56.68, 45.69. ESI-HRMS (*m/z*): Calc. for $M=C_{28}H_{21}N_4O_7Re$: 711.0999 (60%), 713.0994 (100%) $[M + H]^+$. Found: 711.1006 (60%), 713.1050 (100%) $[M + H]^+$.

Synthesis of tricarbonylrheniumbromo(2-phenyl-N-(pyridin-2-ylmethyl)ethanamine), ReL4: $[Re(CO)_5Br]$ (40 mg, 0.1 mmol) and **L4** (21 mg, 0.1 mmol) (synthesis of **L4** is reported in ESI) were dissolved in methanol (3 mL), and the mixture was refluxed for 3 h. The complex crystallized from methanol 1 mL at 4 °C, after 2 days. Yield: 25 mg (45%). Calc. for $C_{17}H_{16}BrN_2O_3Re$: C, 36.30; H, 2.87; N, 4.98; Found: C, 36.59; H, 3.15; N, 4.77. IR (cm⁻¹, KBr): 3448, 3209 (N-H), 2926 (C-H), 2021 (CO), 1913 (CO), 1875 (CO), 1489 (arom. C-C, C-N), 1438 (arom. C-C, C-N). ¹H NMR (500 MHz, CDCl₃, ppm) δ: 8.82 (d, *J* = 5.2 Hz, 1H), 7.84 (t, *J* = 7.8 Hz, 1H), 7.42 (d, *J* = 7.8 Hz, 1H), 7.36–7.23 (m, 6H), 4.71 (dd, *J* = 14.7, 3.9 Hz, 1H), 4.18–4.09 (m, 1H), 3.91–3.89 (m, 1H), 3.70–3.57 (m, 1H), 3.43–3.34 (m, 1H), 3.17–3.01 (m, 2H); ¹³C NMR (126 MHz, CDCl₃, ppm) δ: 196.40 (CO), 195.47 (CO), 191.60 (CO), 158.43, 153.26, 139.02, 136.65, 129.03, 128.80, 127.20, 125.28, 121.96, 60.16, 59.23, 35.11 ESI-HRMS (*m/z*): Calc. for $M=C_{17}H_{16}BrN_2O_3Re$: 481.0685 (60%), 483.0689 (100%) $[M-Br]^+$; 559.0807 (60%), 561.0795 (100%) $[M-Br + DMSO]^+$; Found: 481.0724 (60%), 483.0746 (100%) $[M-Br]^+$; 559.0864 (60%), 561.0893 (100%) $[M-Br + DMSO]^+$.

3.3. X-ray Crystallography of *fac*- $[Re(CO)_3Br(L4)]$

X-ray quality crystals of compound *fac*- $[Re(CO)_3Br(L4)]$ were grown in the mother liquor. A crystal suitable for X-ray diffraction with dimensions 0.14 × 0.09 × 0.07 mm was mounted at rt on a Bruker Kappa APEX2 diffractometer equipped with a triumph monochromator using Mo Kα ($\lambda = 0.71073 \text{ \AA}$, source operating at 50 kV and 30 mA) radiation. Unit cell dimensions were determined and refined using the angular settings of 173 high-intensity reflections ($>10\sigma(I)$) in the range $11 < 2\theta < 36^\circ$. Intensity data were recorded using φ and ω -scans. The crystal remained intact during the data collection. The frames collected were integrated using the Bruker SAINT Software package V7.60A [52], and a narrow-frame algorithm. Data were corrected for absorption using the numerical method (SADABS) based on crystal dimensions [53]. The structure was solved using the SUPERFLIP package [54], incorporated in CRYSTALS. Data refinement (full-matrix least-squares methods on F^2), and all subsequent calculations were carried out using the CRYSTALS version 14.61 build 6236 program package [55–57]. All non-hydrogen atoms were refined anisotropically.

Hydrogen atoms riding on parent carbon atoms were located from difference Fourier maps and refined at idealized positions riding on the parent atoms with isotropic displacement parameters $U_{iso}(H) = 1.2U_{eq}(C)$ or $1.5U_{eq}(\text{methylene and } -\text{NH hydrogens})$ and at distances C–H 0.95 Å and N–H 0.85 Å. All methylene and NH hydrogen atoms were allowed to rotate but not to tip. Illustrations with 50% ellipsoids probability were drawn by CAMERON [58,59]. Crystallographic data for the complex are presented in Table 6.

Table 6. Experimental details.

Crystal Data	
Chemical formula	$C_{17}H_{16}BrN_2O_3Re$
M_r	562.43
Crystal system, space group	Monoclinic, $P2_1/c$
Temperature (K)	295
a, b, c (Å)	11.5730 (8), 20.8663 (11), 7.7637 (5)
β (°)	99.867 (2)
V (Å ³)	1847.1 (2)
Z	4
Radiation type	Mo $K\alpha$
μ (mm ⁻¹)	8.76
Crystal size (mm)	0.14 × 0.09 × 0.07
Data collection	
Diffractometer	Bruker Kappa Apex2
Absorption correction	Numerical Analytical Absorption [56]
T_{min}, T_{max}	0.45, 0.54
No. of measured, independent and observed [$I > 2.0\sigma(I)$] reflections	17060, 3533, 3106
R_{int}	0.029
$(\sin \theta/\lambda)_{max}$ (Å ⁻¹)	0.613
Refinement	
$R[F^2 > 2\sigma(F^2)], wR(F^2), S$	0.036, 0.057, 1.00
No. of reflections	3106
No. of parameters	217
H-atom treatment	H-atom parameters constrained
$\Delta\rho_{max}, \Delta\rho_{min}$ (e Å ⁻³)	1.54, -1.55

Further details on the crystallographic studies as well as atomic displacement parameters are given as Supporting Information in the form of cif files.

Crystallographic data were submitted to the Cambridge Crystallographic Data Center, No. 2374416. Copies of the data are available free of charge upon application to CCDC, 12 Union Road, Cambridge, CB2 1EZ, UK. Telephone: +(44)-1223-336033; E-mail: deposit@ccdc.ac.uk, or via <https://www.ccdc.cam.ac.uk/structures/> (accessed on 30 July 2024).

3.4. DNA-Binding Studies

3.4.1. Study by UV–Vis Spectroscopy

The interaction of the compounds with CT DNA as well as their possible binding modes were investigated by UV–vis spectroscopy and the respective binding constants (K_b) were calculated. The UV–vis spectra of CT DNA were recorded under a constant DNA concentration in the presence of each compound at various mixture ratios (r) [compound]/[DNA]. To obtain the binding constant K_b (in M^{-1}), the changes in the absorbance of each compound at the corresponding λ_{max} of their UV–vis spectra were recorded at increasing CT DNA concentrations (different r values), and it was calculated by the ratio of

slope to the y intercept in plots $[\text{DNA}]/(\varepsilon_A - \varepsilon_f)$ vs. $[\text{DNA}]$, according to the Wolfe–Shimer equation [34]:

$$\frac{[\text{DNA}]}{(\varepsilon_A - \varepsilon_f)} = \frac{[\text{DNA}]}{(\varepsilon_b - \varepsilon_f)} + \frac{1}{K_b(\varepsilon_b - \varepsilon_f)} \quad (1)$$

where $[\text{DNA}]$ is the concentration of DNA in base pairs, $\varepsilon_A = A_{\text{obsd}}/[\text{compound}]$, ε_f = the extinction coefficient of the unbound compound, and ε_b = the extinction coefficient of the compound in the fully bound form.

3.4.2. Viscometry

The viscosity of DNA ($[\text{DNA}] = 0.1 \text{ mM}$) was measured in buffer solution (150 mM NaCl and 15 mM trisodium citrate at pH 7.0) and in increasing amounts of the tested compounds. The measurements were performed at room temperature. The data are presented as $(\eta/\eta_0)^{1/3}$ vs. r , where η is the viscosity of DNA in the presence of the compound, and η_0 is the viscosity of DNA without the compound.

3.4.3. Competition Studies with Ethidium Bromide (EB) via Fluorescence Spectroscopy

The ability of the compounds to displace EB from its DNA–EB complex was investigated by fluorescence emission spectroscopy. The DNA–EB adduct was prepared by mixing 20 μM EB and 26 μM CT DNA in buffer (150mM NaCl and 15mM trisodium citrate at pH 7.0). The intercalating effect of the compounds was studied by adding incremental amounts of the compound into a solution of the DNA–EB adduct. The effect of the addition of each compound to DNA–EB was obtained by measuring the changes of fluorescence emission spectra at the excitation wavelength of 540 nm. The compounds did not exhibit significant fluorescence at rt with or without DNA under the same conditions; therefore, the observed quenching is attributed to the displacement of EB from its EB–DNA adduct. The Stern–Volmer constant (K_{SV}) was employed to evaluate the quenching efficiency of the compounds. The K_{SV} value (in M^{-1}) of the compounds was calculated as the slope of the plot I_0/I vs. $[Q]$, according to the linear Stern–Volmer equation (Equation (2)) [37]:

$$\frac{I_0}{I} = 1 + K_q\tau_0[Q] = 1 + K_{SV}[Q] \quad (2)$$

where I is the emission intensity in the presence of the compound, I_0 is the emission intensity without the presence of the quencher (i.e., the compound under study), K_q = the quenching constant of the EB–DNA system, and τ_0 = the average lifetime of EB–DNA without the quencher. Taking $\tau_0 = 23 \text{ ns}$ as the fluorescence lifetime of the EB–DNA system [38], the EB–DNA quenching constants (K_q , in $\text{M}^{-1}\text{s}^{-1}$) of the compounds were determined from Equation (3) [37]:

$$K_{SV} = K_q \cdot \tau_0 \quad (3)$$

3.5. In Vitro Cell Studies

3.5.1. Cell Cultures

Murine Balb/c colorectal carcinoma CT26 cells were a gift from Prof. C. Chlichlia and were grown in a culture containing DMEM medium that was supplemented with 10% (*v/v*) FBS in the presence of penicillin and streptomycin (1%) at 37 °C and in a humidified atmosphere containing 5% (*v/v*) CO_2 . The medium was renewed every 2 days (<90% confluency in the plates) to allow logarithmic cellular growth in culture. The cells were detached by using trypsin-EDTA solution (25%) (GIBCO Laboratories, Grand Island, NY, USA). The compounds were dissolved in DMSO and then added at the appropriate concentrations in the cell cultures.

3.5.2. Assessment of Proliferation Capacity of CT26 Cells Exposed to Anthrapyrazole Derivatives

The CT26 cells were plated in 24-well plates at a density of 1×10^5 cells/mL. Following the attachment of cells to the plate, the compounds were added in the cultures at various concentrations (10^{-5} – 10^{-7} M). Then, the cells were permitted to grow for an additional 48 h. Subsequently, the cells were detached via trypsinization, and the cell density (number of cells/mL) was measured using a Neubauer chamber. The cell proliferation rate of CT26 cultures was expressed as a percentage (%) of cell growth compared to the control-untreated cell cultures. Furthermore, viability and cellular death were also assessed by using the trypan-blue dye exclusion method.

3.6. ^{99m}Tc Radiochemistry and In Vitro Radiotracer Studies

Synthesis of $^{99m}\text{TcL2}$ and $^{99m}\text{TcL3}$: A fresh solution of *fac*- $[\text{}^{99m}\text{Tc}(\text{CO})_3(\text{H}_2\text{O})_3]^+$ (400 μL , 370–480 MBq) at pH 7 was transferred to a vial containing a methanolic solution of the ligand **L2** or **L3** (50 μL of 10^{-2} M) and an aqueous solution of ascorbic acid (50 μL of 10^{-1} M). The vial was sealed, flushed with N_2 for 5 min and heated at 55–65 $^\circ\text{C}$ for 60 min. The reaction mixtures were analyzed by HPLC. The ^{99m}Tc complexes were purified by HPLC, and after evaporation of the solvents, they were reconstituted in 1% Tween 80 saline solution prior to further study.

Lipophilicity: The lipophilicity of the radiocomplexes was determined by the shake-flask method. $^{99m}\text{TcL2}$ or $^{99m}\text{TcL3}$ (20 μL) were mixed with 2 mL of 1-octanol and 1.98 mL of phosphate buffer (PBS, 0.1 M, pH 7.4) in a centrifuge tube. The mixture was vortexed at rt for 1 min and centrifuged at 3500 rpm for 5 min. Aliquots (50 μL) of both 1-octanol and PBS phases were withdrawn and counted in a gamma counter. The experiment was conducted in triplicates. The distribution coefficient (D) was calculated by dividing the radioactivity of the organic phase with that of the aqueous phase, and the results are expressed as $\log D_{7.4}$.

Stability studies: Histidine challenge: The purified $^{99m}\text{TcL2}$ or $^{99m}\text{TcL3}$ (50 μL , approx. 11–15 MBq) was mixed with a solution of L-histidine (1 mM) in 0.1 M PBS, pH 7.4 (0.45 mL) and incubated at 37 $^\circ\text{C}$ for 4 h. The mixtures were analyzed by HPLC at 1 and 4 h.

Rat plasma stability: $^{99m}\text{TcL2}$ or $^{99m}\text{TcL3}$ (100–120 μL , 25–30 MBq) was mixed with undiluted rat plasma (0.5 mL) at 37 $^\circ\text{C}$ for 4 h. Samples were withdrawn at 1 and 4 h, which were mixed with three times the volume of acetonitrile, to precipitate the proteins. The mixture was centrifuged at 5000 rpm for 10 min and the supernatant solution was separated from the solids. The radioactivity of the solution and the solid was measured in a γ -counter, and the solution was analyzed by HPLC.

Cellular uptake of $^{99m}\text{TcL2}$ and $^{99m}\text{TcL3}$: The CT26 cells were seeded at a density of 1×10^6 cells/mL in 24-well plates and were allowed to attach for 6 h. Aliquots of $^{99m}\text{TcL2}$ or $^{99m}\text{TcL3}$ (20–40 μL , 0.9 MBq) were added to each plate and the cells were incubated for 15, 60, 120, and 240 min at 37 $^\circ\text{C}$ in an atmosphere containing 5% (*v/v*) CO_2 . The culture medium was withdrawn and the cells were detached using trypsin-EDTA (200 μL 0.25% *w/v*). After 2 min incubation, DMEM was added in the culture. The solution containing the cells was transferred to a tube followed by centrifugation, (5 min, 2000 rpm) and the cells were washed with $1 \times$ PBS twice (150 and 120 μL). The radioactivity of the cells and supernatant was counted in γ -counter to evaluate the cellular uptake. The experiment was conducted in triplicates for each time point.

3.7. Biodistribution Studies of $^{99m}\text{TcL2}$ in Mice

The experiment was approved by the Aristotle University Committee for Animal Experimentation (License No 114251/528), and was performed according to the European guidelines 2010/63/EU and Greek legislation (PD 56) for animal experimentation. Balb/c mice, 10–12 weeks old, with a median weight of 20–25 g, were housed in suitable animal facilities (Laboratory of Development-Breeding of Animal Models and Biomedical Research, Faculty of Health Sciences, Aristotle University, EU License No EL 54 BIOexp-10) with food and water ad libitum and constant conditions of temperature, humidity and regular light

cycles of 12/12 h light/dark. The 3R alternatives (Replacement, Refinement, Reduction) were considered in all animal experiments, while the mice were not subjected to pain or discomfort during the experimentation.

Balb/c were implanted subcutaneously with 5×10^6 CT26 cells on the hind right flank. One week after inoculation, when the tumor size was between 0.4–1 cm, the animals were injected in the tail vein with ~370 kBq of the HPLC-purified tracer $^{99m}\text{TcL2}$ in 0.1 mL saline each. Animals were sacrificed at 30 and 120 min post-injection (p.i.) by cervical dislocation, which was followed by blood withdrawal and myocardial excision. Organs and tissues of interest were excised and weighed, and their radioactivity was measured by a γ scintillator. The radioactivity of the samples was decay-corrected by the use of a standard solution corresponding to 1% of the injected dose. The radioactivity of the tissues and organs is expressed as a percentage of the injected dose per gram tissue (% ID/g). Values are quoted as the mean% ID \pm standard deviation (SD) of the four mice per group. Blood volume and muscle mass were estimated at 7 and 43% of body weight, respectively.

4. Conclusions

In this work, three new anthrapyrazole ligands and their respective tricarbonylrhenium complexes were synthesized and characterized. All compounds possess the ability to intercalate with DNA. Complex **ReL1** acts as a metallointercalator with strong DNA-binding affinity. However, it was not cytotoxic at the tested concentration range and cell line, which is attributed to the ligand's N-substituent. The anthrapyrazole pendant complexes **ReL2** and **ReL3** show strong DNA-binding affinities, with **ReL3** exhibiting the highest DNA-binding constant among the tested compounds. Tumor cell cytotoxicity was high for ligand **L2** and complex **ReL2** with submicromolar IC_{50} values of 0.36 and 0.64 μM , respectively. The low cytotoxicity of **ReL3** can be attributed also to its low cell uptake, based on the radiotracer studies with its analogous $^{99m}\text{TcL3}$. As complex **ReL2** was the most cytotoxic, its γ -emitting analogue $^{99m}\text{TcL2}$ was evaluated for its tumor cell uptake and biodistribution properties in tumor-bearing mice. It was observed that this tracer exhibits high tumor uptake in vitro as well as accumulation in the tumor in vivo. **ReL2** is a cytotoxic DNA-intercalator with suitable pharmacokinetic properties to be distributed in tumors in vivo and may be considered for further studies. Also, future design should focus on compounds with suitable substituents which is critical for cytotoxicity.

Supplementary Materials: The following supporting information can be downloaded at: <https://www.mdpi.com/article/10.3390/inorganics12090254/s1>, 1. Synthesis of Ligand **L4**; 2. NMR spectra of **L1-L4** and **ReL1-ReL4**; 3. IR spectra; Figure S1: ORTEP diagram of the S enantiomer of **ReL4**; Table S1: Computed octahedral distortion parameters; Figure S2: UV-vis spectra of DMSO solution of **L1, L2, ReL1** and **ReL2** in the presence of increasing amounts of CT DNA; Figure S3: Plot of $([\text{DNA}]) / (\epsilon_A - \epsilon_f)$ versus $[\text{DNA}]$ for compounds **L1-L3** and **ReL1-ReL3**. Figure S4: Fluorescence emission spectra of compounds **L1-L3** and **ReL1-ReL2**; Figure S5: Stern–Volmer quenching plot of EB–DNA fluorescence for compounds **L1-L3** and **ReL1-ReL3**; Figure S6: IC_{50} curve of **L2** and **ReL2**. Figure S7: HPLC analysis of **L2, ReL2, ReL2'** and $^{99m}\text{TcL2}$.

Author Contributions: Conceptualization, D.P. and G.P. (Georgios Papparidis); methodology, G.P. (George Psomas), I.S.V., A.H. and C.G.; resources, D.S., I.S.V., G.P. (George Psomas) and D.P.; data curation, G.P. (Georgios Papparidis) and M.A.; writing—original draft preparation, G.P. (Georgios Papparidis), G.P. (George Psomas), I.S.V. and A.H.; writing—review and editing, D.P.; supervision, D.P., I.S.V. and G.P. (George Psomas). All authors have read and agreed to the published version of the manuscript.

Funding: This research received no external funding.

Institutional Review Board Statement: The experiment was approved by the Aristotle University Committee for Animal Experimentation (License No 114251/528), and was performed according to the European guidelines 2010/63/EU and Greek legislation (PD 56) for animal experimentation.

Data Availability Statement: The data of this work are provided within the manuscript and in the Supplementary Materials.

Acknowledgments: The authors are grateful to I. Iakovou, Head of the AHEPA Hospital Nuclear Medicine Laboratory, for donating ^{99m}Tc to perform the study.

Conflicts of Interest: The authors declare no conflicts of interest.

References

1. Muhammad, N.; Guo, Z. Metal-Based Anticancer Chemotherapeutic Agents. *Curr. Opin. Chem. Biol.* **2014**, *19*, 144–153. [[CrossRef](#)]
2. Ye, R.; Tan, C.; Chen, B.; Li, R.; Mao, Z. Zinc-Containing Metalloenzymes: Inhibition by Metal-Based Anticancer Agents. *Front. Chem.* **2020**, *8*, 402. [[CrossRef](#)]
3. Simpson, P.V.; Desai, N.M.; Casari, I.; Massi, M.; Falasca, M. Metal-Based Antitumor Compounds: Beyond Cisplatin. *Future Med. Chem.* **2019**, *11*, 119–135. [[CrossRef](#)]
4. Wernitznig, D.; Kiakos, K.; Del Favero, G.; Harrer, N.; Machat, H.; Osswald, A.; Jakupec, M.A.; Wernitznig, A.; Sommergruber, W.; Keppler, B.K. First-in-Class Ruthenium Anticancer Drug (KP1339/IT-139) Induces an Immunogenic Cell Death Signature in Colorectal Spheroids in Vitro. *Metallomics* **2019**, *11*, 1044–1048. [[CrossRef](#)]
5. King, A.P.; Wilson, J.J. Endoplasmic Reticulum Stress: An Arising Target for Metal-Based Anticancer Agents. *Chem. Soc. Rev.* **2020**, *49*, 8113–8136. [[CrossRef](#)]
6. Anthony, E.J.; Bolitho, E.M.; Bridgewater, H.E.; Carter, O.W.L.; Donnelly, J.M.; Imberti, C.; Lant, E.C.; Lermyte, F.; Needham, R.J.; Palau, M.; et al. Metallodrugs Are Unique: Opportunities and Challenges of Discovery and Development. *Chem. Sci.* **2020**, *11*, 12888–12917. [[CrossRef](#)]
7. Ortega, E.; Viguera, G.; Ballester, F.J.; Ruiz, J. Targeting Translation: A Promising Strategy for Anticancer Metallodrugs. *Coord. Chem. Rev.* **2021**, *446*, 214129. [[CrossRef](#)]
8. Ghosh, S. Cisplatin: The First Metal Based Anticancer Drug. *Bioorg. Chem.* **2019**, *88*, 102925. [[CrossRef](#)]
9. Clède, S.; Lambert, F.; Saint-Fort, R.; Plamont, M.A.; Bertrand, H.; Vessières, A.; Policar, C. Influence of the Side-Chain Length on the Cellular Uptake and the Cytotoxicity of Rhenium Tricarbonyl Derivatives: A Bimodal Infrared and Luminescence Quantitative Study. *Chem. A Eur. J.* **2014**, *20*, 8714–8722. [[CrossRef](#)] [[PubMed](#)]
10. Leonidova, A.; Pierroz, V.; Adams, L.A.; Barlow, N.; Ferrari, S.; Gra, B. Enhanced Cytotoxicity through “Click” Conjugation of a Luminescent Re (I) Complex to a Cell-Penetrating Lipopeptide. *ACS Med. Chem. Lett.* **2014**, *5*, 809–814. [[CrossRef](#)] [[PubMed](#)]
11. Leonidova, A.; Pierroz, V.; Rubbiani, R.; Heier, J.; Ferrari, S.; Gasser, G. Towards Cancer Cell-Specific Phototoxic Organometallic Rhenium (I) Complexes. *Dalton Trans.* **2014**, *43*, 4287–4294. [[CrossRef](#)] [[PubMed](#)]
12. Knopf, K.M.; Murphy, B.L.; Macmillan, S.N.; Baskin, J.M.; Barr, M.P.; Boros, E.; Wilson, J.J. In Vitro Anticancer Activity and in Vivo Biodistribution of Rhenium (I) Tricarbonyl Aqua Complexes. *J. Am. Chem. Soc.* **2017**, *139*, 14302–14314. [[CrossRef](#)] [[PubMed](#)]
13. Schindler, K.; Zobi, F. Anticancer and Antibiotic Rhenium Tri- and Dicarbonyl Complexes: Current Research and Future Perspectives. *Molecules* **2022**, *27*, 539. [[CrossRef](#)] [[PubMed](#)]
14. Rescifina, A.; Zagni, C.; Varrica, M.G.; Pistarà, V.; Corsaro, A. Recent Advances in Small Organic Molecules as DNA Intercalating Agents: Synthesis, Activity, and Modeling. *Eur. J. Med. Chem.* **2014**, *74*, 95–115. [[CrossRef](#)] [[PubMed](#)]
15. Liu, H.-K.; Sadler, P.J. Metal Complexes as DNA Intercalators. *Acc. Chem. Res.* **2011**, *44*, 349–359. [[CrossRef](#)]
16. Lee, L.C.-C.; Leung, K.-K.; Lo, K.K.-W. Recent Development of Luminescent Rhenium (I) Tricarbonyl Polypyridine Complexes as Cellular Imaging Reagents, Anticancer Drugs, and Antibacterial Agents. *Dalton Trans.* **2017**, *46*, 16357–16380. [[CrossRef](#)]
17. Pagoni, C.C.; Xylouri, V.S.; Kaiafas, G.C.; Lazou, M.; Bompola, G.; Tsoukas, E.; Papadopoulou, L.C.; Psomas, G.; Papa- giannopoulou, D. Organometallic Rhenium Tricarbonyl—Enrofloxacin and—Levofloxacin Complexes: Synthesis, Albumin— Binding, DNAi—Interaction and Cell Viability Studies. *JBIC J. Biol. Inorg. Chem.* **2019**, *24*, 609–619. [[CrossRef](#)]
18. Nasiri Sovari, S.; Kolly, I.; Schindler, K.; Djuric, A.; Srdic-Rajic, T.; Crochet, A.; Pavic, A.; Zobi, F. Synthesis, Characterization, and in Vivo Evaluation of the Anticancer Activity of a Series of 5- and 6-(Halomethyl)-2,2'-Bipyridine Rhenium Tricarbonyl Complexes. *Dalton Trans.* **2023**, *52*, 6934–6944. [[CrossRef](#)]
19. Frederick, C.A.; Williams, L.D.; Ughetto, G.; Van der Marel, G.A.; Van Boom, J.H.; Rich, A.; Wang, A.H.J. Structural Comparison of Anticancer Drug-DNA Complexes: Adriamycin and Daunomycin. *Biochemistry* **1990**, *29*, 2538–2549. [[CrossRef](#)]
20. Mattioli, R.; Ilari, A.; Colotti, B.; Mosca, L.; Fazi, F.; Colotti, G. Doxorubicin and Other Anthracyclines in Cancers: Activity, Chemoresistance and Its Overcoming. *Mol. Asp. Med.* **2023**, *93*, 101205. [[CrossRef](#)]
21. Imstepf, S.; Pierroz, V.; Rubbiani, R.; Felber, M.; Fox, T.; Gasser, G.; Alberto, R. Organometallic Rhenium Complexes Divert Doxorubicin to the Mitochondria. *Angew. Chem. Int. Ed.* **2016**, *55*, 2792–2795. [[CrossRef](#)]
22. Cardinale, D.; Iacopo, F.; Cipolla, C.M. Cardiotoxicity of Anthracyclines. *Front. Cardiovasc. Med.* **2020**, *7*, 26. [[CrossRef](#)]
23. Gogas, H.; Mansi, J.L. New Drugs. The Anthracyclines. *Cancer Treat. Rev.* **1996**, *21*, 541–552. [[CrossRef](#)] [[PubMed](#)]
24. Tan, J.H.; Zhang, Q.X.; Huang, Z.S.; Chen, Y.; Wang, X.D.; Gu, L.Q.; Wu, J.Y. Synthesis, DNA Binding and Cytotoxicity of New Pyrazole Emodin Derivatives. *Eur. J. Med. Chem.* **2006**, *41*, 1041–1047. [[CrossRef](#)] [[PubMed](#)]
25. Haiyang, H.; Morley, J.E.; Twamley, B.; Groeneman, R.H.; Bucar, D.K.; MacGillivray, L.R.; Benny, P.D. Investigation of the Coordination Interactions of S-(Pyridin-2-Ylmethyl)-L-Cysteine Ligands with $\text{M}(\text{CO})_3^+$ (M = Re, ^{99m}Tc). *Inorg. Chem.* **2009**, *48*, 10625–10634.

26. Makris, G.; Radford, L.; Gallazzi, F.; Jurisson, S.; Hennkens, H.; Papagiannopoulou, D. Synthesis and Evaluation of fac-[^{99m}Tc/Re(CO)₃]⁺ Complexes with a New (N,S,N) Bifunctional Chelating Agent: The First Example of a fac-[Re(CO)₃(N,S,N-Sst2-ANT)] Complex Bearing a Somatostatin Receptor Antagonist Peptide. *J. Organomet. Chem.* **2016**, *805*, 100–107. [[CrossRef](#)]
27. He, H.; Lipowska, M.; Xu, X.; Taylor, A.T.; Marzilli, L.G. Rhenium Analogues of Promising Renal Imaging Agents with a {^{99m}Tc(CO)₃}⁺ Core Bound to Cysteine-Derived Dipeptides, Including Lanthionine. *Inorg. Chem.* **2007**, *46*, 590–596. [[CrossRef](#)]
28. Suárez-Ortiz, G.A.; Hernández-Correa, R.; Morales-Moreno, M.D.; Toscano, R.A.; Ramirez-Apan, M.T.; Hernandez-Garcia, A.; Amézquita-Valencia, M.; Araiza-Olivera, D. Diastereomeric Separation of Chiral Fac-Tricarbonyl (Iminopyridine) Rhenium (I) Complexes and Their Cytotoxicity Studies: Approach toward an Action Mechanism against Glioblastoma. *J. Med. Chem.* **2022**, *65*, 9281–9294. [[CrossRef](#)]
29. Song, X.; Lim, M.H.; Mohamed, D.K.B.; Wong, S.M.; Zhao, J.; Hor, T.S.A. Re (I) Carbonyl Complexes Containing Pyridyl-Imine and Amine Ligands: Synthesis, Characterization and Their Catalytic Olefin Epoxidation Activities. *J. Organomet. Chem.* **2016**, *814*, 1–7. [[CrossRef](#)]
30. Saund, S.S.; Siegler, M.A.; Thoi, V.S. Electrochemical Degradation of a Dicationic Rhenium Complex via Hoffman-Type Elimination. *Inorg. Chem.* **2021**, *60*, 13011–13020. [[CrossRef](#)]
31. Liu, W.; Heinze, K. Rhenium (I) and Platinum (II) Complexes with Diimine Ligands Bearing Acidic Phenol Substituents: Hydrogen-Bonding, Acid–Base Chemistry and Optical Properties. *Dalton Trans.* **2010**, *39*, 9554–9564. [[CrossRef](#)] [[PubMed](#)]
32. Wang, W.; Spingler, B.; Alberto, R. Reactivity of 2-Pyridine–Aldehyde and 2-Acetyl–Pyridine Coordinated to [Re(CO)₃]⁺ with Alcohols and Amines: Metal Mediated Schiff Base Formation and Dimerization. *Inorganica Chim. Acta* **2003**, *355*, 386–393. [[CrossRef](#)]
33. Ketkaew, R.; Tantirungrotechai, Y.; Harding, P.; Chastanet, G.; Guionneau, P.; Marchivie, M.; Harding, D.J. OctaDist: A Tool for Calculating Distortion Parameters in Spin Crossover and Coordination Complexes. *Dalton Trans.* **2021**, *50*, 1086–1096. [[CrossRef](#)]
34. Wolfe, A.; Shimer, G.; Meehan, T. Polycyclic Aromatic Hydrocarbons Physically Intercalate into Duplex Regions of Denatured DNA. *Biochemistry* **1987**, *26*, 6392–6396. [[CrossRef](#)] [[PubMed](#)]
35. Zhao, G.; Lin, H.; Zhu, S.; Sun, H.; Chen, Y. Dinuclear Palladium (II) Complexes Containing Two Monofunctional [Pd(En)(Pyridine)Cl]⁺ Units Bridged by Se or S. Synthesis, Characterization, Cytotoxicity and Kinetic Studies of DNA-Binding. *J. Inorg. Biochem.* **1998**, *70*, 219–226. [[CrossRef](#)]
36. Luis García-Giménez, J.; González-Álvarez, M.; Liu-González, M.; Macías, B.; Borrás, J.; Alzuet, G. Toward the Development of Metal-Based Synthetic Nucleases: DNA Binding and Oxidative DNA Cleavage of a Mixed Copper (II) Complex with N-(9H-Purin-6-Yl) Benzenesulfonamide and 1,10-Phenanthroline. Antitumor Activity in Human Caco-2 Cells and Jurkat T Lymphocy. *J. Inorg. Biochem.* **2009**, *103*, 923–934. [[CrossRef](#)]
37. Lakowicz, J.R. *Principles of Fluorescence Spectroscopy*, 3rd ed.; Plenum Press: New York, NY, USA, 2006.
38. Wilson, W.D.; Ratmeyer, L.; Zhao, M.; Streckowski, L.; Boykin, D. The Search for Structure-Specific Nucleic Acid-Interactive Drugs: Effects of Compound Structure on RNA versus DNA Interaction Strength. *Biochemistry* **1993**, *32*, 4098–4104. [[CrossRef](#)] [[PubMed](#)]
39. Heller, D.P.; Greenstock, C.L. Fluorescence Lifetime Analysis of DNA Intercalated Ethidium Bromide and Quenching by Free Dye. *Biophys. Chem.* **1994**, *50*, 305–312. [[CrossRef](#)]
40. Sharma, A.; Özayral, S.; Caserto, J.S.; ten Cate, R.; Anders, N.M.; Barnett, J.D.; Kandala, S.K.; Henderson, E.; Stewart, J.; Liapi, E.; et al. Increased Uptake of Doxorubicin by Cells Undergoing Heat Stress Does Not Explain Its Synergistic Cytotoxicity with Hyperthermia. *Int. J. Hyperth.* **2019**, *36*, 712–720. [[CrossRef](#)]
41. Shimolina, L.E.; Gulin, A.A.; Paez-Perez, M.; López-Duarte, I.; Druzhkova, I.N.; Lukina, M.M.; Gubina, M.V.; Brooks, N.J.; Zagaynova, E.V.; Kuimova, M.K.; et al. Mapping Cisplatin-Induced Viscosity Alterations in Cancer Cells Using Molecular Rotor and Fluorescence Lifetime Imaging Microscopy. *J. Biomed. Opt.* **2020**, *25*, 126004. [[CrossRef](#)]
42. Showalter, H.D.; Johnson, J.L.; Hoftiezer, J.M.; Turner, W.R.; Werbel, L.M.; Leopold, W.R.; Shillis, J.L.; Jackson, R.C.; Elslager, E.F. Anthrapyrazole Anticancer Agents. Synthesis and Structure-Activity Relationships against Murine Leukemias. *J. Med. Chem.* **1987**, *30*, 121–131. [[CrossRef](#)] [[PubMed](#)]
43. Kostakis, I.K.; Magiatis, P.; Pouli, N.; Marakos, P.; Skaltsounis, A.L.; Pratsinis, H.; Léonce, S.; Pierré, A. Design, Synthesis, and Antiproliferative Activity of Some New Pyrazole-Fused Amino Derivatives of the Pyranoxanthene, Pyranothioxanthene, and Pyranoacridone Ring Systems: A New Class of Cytotoxic Agents. *J. Med. Chem.* **2002**, *45*, 2599–2609. [[CrossRef](#)] [[PubMed](#)]
44. Zee-Cheng, R.K.Y.; Podrebarac, E.G.; Menon, C.S.; Cheng, C.C. Structural Modification Study of Bis (Substituted Aminoalkylamino) Anthraquinones. An Evaluation of the Relationship of the [2-[(2-Hydroxyethyl)Amino]Ethyl] Amino Side Chain with Antineoplastic Activity. *J. Med. Chem.* **1979**, *22*, 501–505. [[CrossRef](#)]
45. Papagiannopoulou, D. Technetium-99m Radiochemistry for Pharmaceutical Applications. *J. Label. Comp. Radiopharm.* **2017**, *60*, 502–520. [[CrossRef](#)] [[PubMed](#)]
46. Schmidt, S.; Trogler, W.; Basolo, F. Pentacarbonyl Rhenium Halides. *Inorg. Synth.* **1985**, *23*, 41.
47. Nitschke, J.; Schmidt, S.P.; Trogler, W.C. Properties of (Trifluoromethanesulfonato) Pentacarbonylmanganese (I) and Rhenium (I). Reactions in Superacid Solvents. *Inorg. Chem.* **1985**, *24*, 1972–1978. [[CrossRef](#)]
48. Alberto, R.; Schibli, R.; Egli, A.; Schubiger, A.P.; Abram, U.; Kaden, T.A. A Novel Organometallic Aqua Complex of Technetium for the Labeling of Biomolecules: Synthesis of [^{99m}Tc(OH₂)₃(CO)₃]⁺ from [^{99m}TcO₄][−] in Aqueous Solution and Its Reaction with a Bifunctional Ligand. *J. Am. Chem. Soc.* **1998**, *120*, 7987–7988. [[CrossRef](#)]

49. Marmur, J. A Procedure for the Isolation of Deoxyribonucleic Acid from Micro-Organisms. *J. Mol. Biol.* **1961**, *3*, 208-IN1. [[CrossRef](#)]
50. Reichmann, M.E.; Rice, S.; Thomas, C.; Doty, P. A Further Examination of the Molecular Weight and Size of Desoxypentose Nucleic Acid. *J. Am. Chem. Soc.* **1954**, *76*, 3047–3053. [[CrossRef](#)]
51. Policar, C.; Lambert, F.; Cesario, M.; Morgenstern-Badarau, I. An Inorganic Helix $[\text{Mn}(\text{IPG})(\text{MeOH})]_n[\text{PF}_6]_n^{\text{[†]}}$: Structural and Magnetic Properties of a Syn-Anti Carboxylate-Bridged Manganese (II) Chain Involving a Tetradentate Ligand. *Eur. J. Inorg. Chem.* **1999**, *1999*, 2201–2207. [[CrossRef](#)]
52. McInally, C. *Apex2*; Bruker Analytical X-Ray Systems, Inc.: Madison, WI, USA, 2006; p. M86-E01078.
53. Sheldrick, G.M. *SADABS: Area-Detector Absorption Correction*; Siemens Industrial Automation, Inc.: Madison, WI, USA, 1996.
54. Palatinus, L.; Chapuis, G. SUPERFLIP—A computer program for the solution of crystal structures by charge flipping in arbitrary dimensions. *J. Appl. Crystallogr.* **2007**, *40*, 786–790. [[CrossRef](#)]
55. Betteridge, P.W.; Carruthers, J.R.; Cooper, R.I.; Prout, K.; Watkin, D.J. CRYSTALS version 12: Software for guided crystal structure analysis. *J. Appl. Crystallogr.* **2003**, *36*, 1487. [[CrossRef](#)]
56. Watkin, D. The Control of Difficult Refinements. *Acta Crystallogr. Sect. A* **1994**, *50*, 411–437. [[CrossRef](#)]
57. Prince, E. *Mathematical Techniques in Crystallography and Materials Science*; Springer: Berlin/Heidelberg, Germany, 1982.
58. Watkin, D.J.; Prout, C.K.; Pearce, L.J. CAMERON, *Chemical Crystallography Laboratory*; University of Oxford: Oxford, UK, 1996.
59. De Meulenaer, J.; Tompa, H. The Absorption Correction in Crystal Structure Analysis. *Acta Crystallogr.* **1965**, *19*, 1014–1018. [[CrossRef](#)]

Disclaimer/Publisher's Note: The statements, opinions and data contained in all publications are solely those of the individual author(s) and contributor(s) and not of MDPI and/or the editor(s). MDPI and/or the editor(s) disclaim responsibility for any injury to people or property resulting from any ideas, methods, instructions or products referred to in the content.